NIST Technical Note 1441

Phase Composition Analysis of the NIST Reference Clinkers by Optical Microscopy and X-ray Powder Diffraction

Paul Stutzman

Stefan Leigh

NIST National Institute of Standards and Technology • Technology Administration • U.S. Department of Commerce

NIST Technical Note 1441

Phase Composition Analysis of the NIST Reference Clinkers by Optical Microscopy and X-ray Powder Diffraction

Paul Stutzman
Building and Fire Research Laboratory
Stefan Leigh
Statistical Engineering Laboratory

September 2002

U.S. Department of Commerce
Donald L. Evans, Secretary

Technology Administration

Phillip J. Bond, Under Secretary for Technology

Certain commercial entities, equipment, or materials may be identified in this document in order to describe an experimental procedure or concept adequately. Such identification is not intended to imply recommendation or endorsement by the National Institute of Standards and Technology, nor is it intended to imply that the entities, materials, or equipment are necessarily the best available for the purpose.

National Institute of Standards and Technology Technical Note 1441
Natl. Inst. Stand. Technol. Tech. Note 1441, 44 pages (September 2002)
CODEN: NSPUE2

U.S. GOVERNMENT PRINTING OFFICE
WASHINGTON: 2002

For sale by the Superintendent of Documents, U.S. Government Printing Office
Internet: bookstore.gpo.gov — Phone: (202) 512-1800 — Fax: (202) 512-2250
Mail: Stop SSOP, Washington, DC 20402-0001

Abstract

Certification of the phase compositions of the three NIST Reference Clinkers will be based upon more than one independent method. The current reference values were established using an optical microscope examination, with additional optical microscope data taken from an ASTM C 1356 round robin. The present X-ray powder diffraction (XRD) study provides a second, independent estimate of the phase abundance. Reitveld refinement of the powder diffraction data allowed calculation of a set of best-fit reference patterns and their scale factors. Because of significant contrast in the linear absorption coefficients of ferrite and periclase relative to the estimated mean matrix linear absorption coefficient, the scale factors were adjusted for microabsorption effects. The XRD data generally agree with the optical data with the exception of aluminate. This disagreement may reflect the difficulty in resolving this fine-sized phase using the optical microscope. The XRD data show greater precision than replicate measurements by microscopy.

Measurements from different sources, laboratories, instruments, and methods can exhibit significant between-method variability, as well as distinct within-method variances. The data sets were analyzed using both unweighted and weighted schemes to establish optimal consensus values and to provide meaningful consensus uncertainties. While the consensus mean values of individual phase abundance do not vary significantly across methods of combining data sources, the associated uncertainty values do. The Mandel-Paule-Vangel-Rukhin maximum likelihood method of combining the data sets is favored as this method produces a weighted mean whose weighting scheme does not necessarily skew the consensus value in the direction of the large number of XRD values, and it takes between- as well as within-method variation explicitly into account.

Table of Contents

List of Tables

List of Figures

Introduction

Improvements in cement production and prediction of cements' performance properties require the application of material science, which, in turn, requires the ability to determine and describe their micro- and macrostructures. Improved methods for determining the phase composition of cements using X-ray powder diffraction will facilitate this understanding. This project, part of the Partnership for High-Performance Concrete Technology at the National Institute of Standards and Technology (NIST), involves the development and testing of analytical methods necessary for characterization of cements. Rietveld refinements to model the complex X-ray powder diffraction (XRD) patterns of cementitious materials will provide phase, chemical, and structural information in order to more completely characterize them, and so provide an improved basis for investigating relationships among cement properties and performance properties.

RMs 8486, 8487, and 8488 are three NIST reference clinkers used for developing and testing methods of quantitative phase analysis [1]. These clinkers were selected as representative of the range of North American clinker production with respect to phase abundance, crystal size, and crystal distribution. The reference values are currently based upon an optical microscope examination of polished, etched sections. The XRD study is intended to provide both an additional estimate using an independent method of analysis, and data to examine inter- and intra- sample heterogeneity. The combined XRD and optical datasets are used to establish the certified values.

Reflected light microscopy images illustrate the textures of the three clinkers. Epoxy-impregnated, polished specimens are etched with hydrofluoric acid vapor to facilitate phase identification. Alite is colored brown and belite, blue to brown. Distinguishing features of the silicate phases are the hexagonal crystal outline of alite, and the rounded form and internal lameller structure of belite. Ferrite appears white due to its high reflectivity and occurs in both a lath-like or dendritic forms. Aluminate appears gray and is often found with the ferrite; both of which are sometimes referred to as the interstitial phases. Periclase appears gray and is identified by its equant crystal habit and size.

Clinker 8486 (Figure 1) is intermediate in crystal size and exhibits heterogeneous phase distribution relative to the other clinkers. Alite appears as brown subhedral to anhedral crystals approximately 25μm in size. Belite occurs in large clusters, as rounded crystals about 15μm in diameter, which often exhibits the internal lameller structure. Ferrite occurs as medium- to fine-grained lath-like crystals that appear white. Aluminate as gray crystals between the ferrite crystals, and periclase occurs as gray, equant crystals up to 15μm in both the matrix and within some alite crystals.

Clinker 8487 (Figure 2) exhibits a fine crystal size and relatively homogeneous phase distribution, with the exception of belite and free lime, which both occur as clusters within the microstructure. Alite occurrs as anhedral grains approximately 12μm and comprises the bulk of the clinker. The matrix contains subhedral aluminate and fine-grained ferrite. Some of the ferrite is intimately intermixed with the aluminate. Some of the pores contain alkali sulfates. This clinker may be difficult to examine microscopically because of the fine texture of the aluminate and ferrite and the uneven distribution of the belite and free lime.

Clinker 8488 (Figure 3) is the most coarsely crystalline of the three clinkers and exhibits the most homogeneous distribution of the constituent phases. Subhedral to anhedral alite crystals up to 110μm form the bulk of the clinker. Belite occurs as rounded, evenly distributed crystals of about 35μm diameter. Ferrite occurs with both lath-like and dendritic habit while aluminate crystals may be found between ferrite crystals.

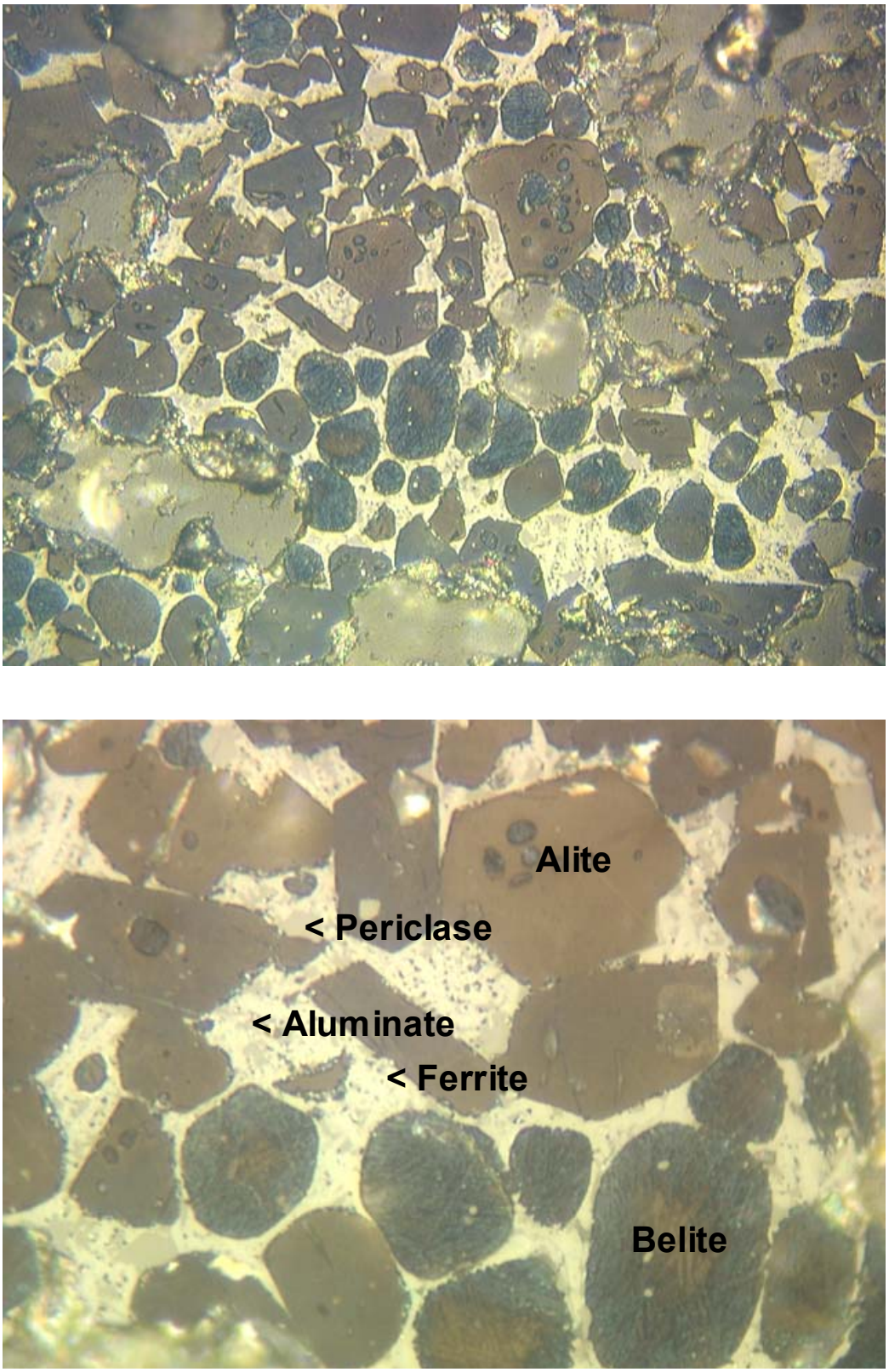

Figure 1: RM 8486 polished section prepared using a 30 s HF vapor etch with a field width of 260µm (upper) and 100µm (lower image).

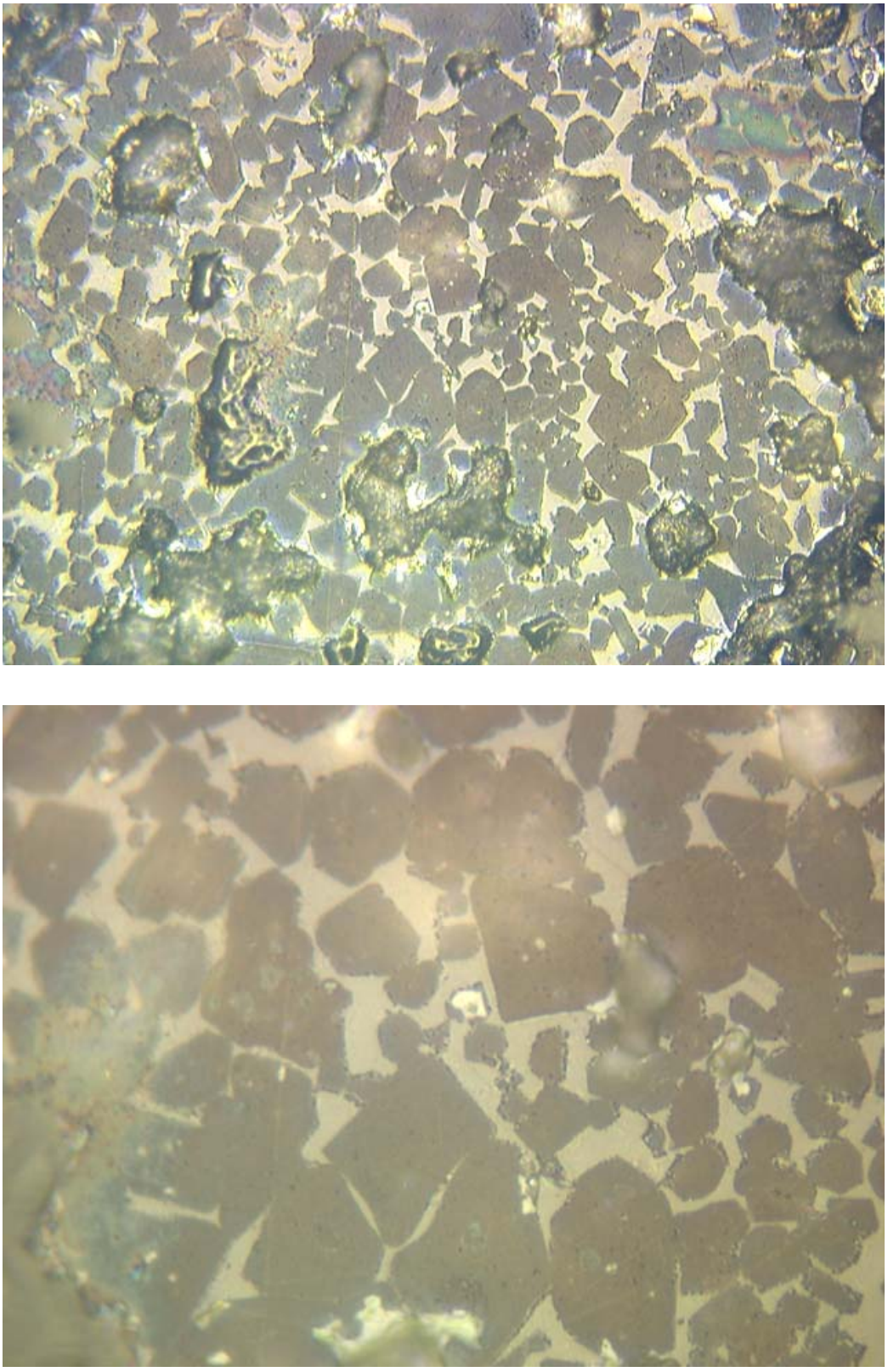

Figure 2: RM 8487 polished section prepared using a 30 s HF vapor etch with a field width of 260µm (upper) and 100µm (lower image).

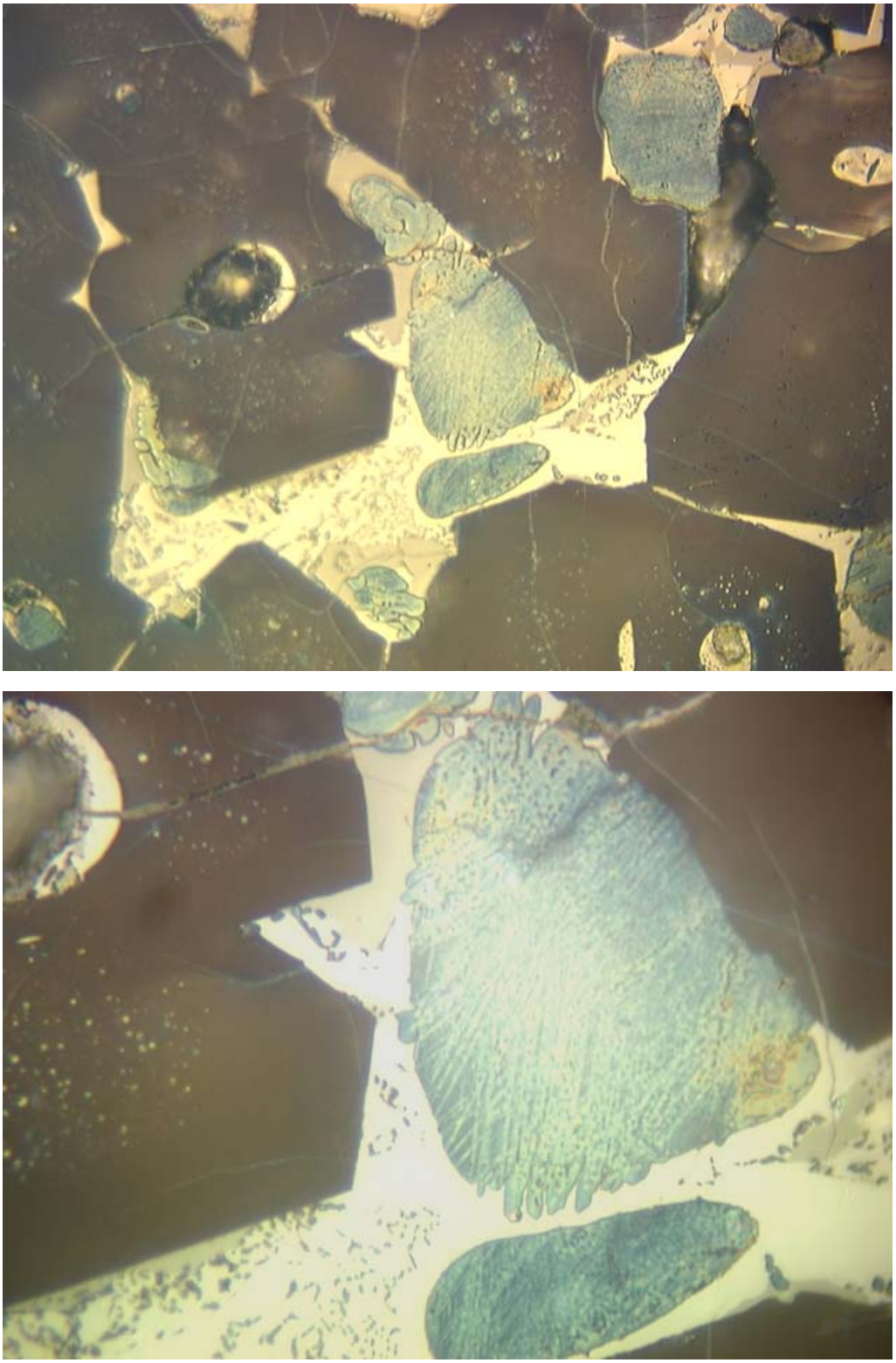

Figure 3: RM 8488 polished section prepared using a 30 s HF vapor etch with a field width of 260µm (upper) and 100µ m (lower image).

Microscopical Analysis

Clinker petrography has long been used in the examination of clinker materials. ASTM 1356M [2] provides guidance in phase abundance analysis using a microscopical point-count procedure. The original certificate phase abundance estimates were performed using a procedure similar to that of ASTM 1356M while the round robin data were collected following that ASTM standard test method. The advantages of optical microscopy (OM) over chemical analyses are that it provides direct examination of the clinker, characterization of both phase composition and texture, and a rapid, relatively simple method for estimating the phase volume fraction via point count analysis. Procedures for preparation and examination of clinker may be found in Campbell [3].

X-Ray Powder Diffraction

XRD analysis of clinker has been used in cement studies for the past 60 years, and applied in phase abundance analysis over the past 40 years. ASTM 1365 [4] details a standard test method for quantitative phase abundance analysis using XRD for determination of ferrite, aluminate, and periclase (QXRD)**.** XRD is a direct, bulk analysis technique where the patterns provide phase, chemical and crystal structure information data that may afford greater understanding of cement property/performance relationships. However, XRD analysis of clinker has proven difficult as the multiple phases result in substantial peak overlap. There is also difficulty in securing suitable pure phase reference standards. These concerns may be addressed using the Rietveld method for X-ray powder diffraction [5]. Public domain code General Structure Analysis System (GSAS) can be used to refine the powder diffraction data [6].

The Rietveld method allows standardization of powder diffraction analysis through use of calculated reference diffraction patterns based upon crystal structure models (Fig. 4). The result is a set of refined crystal structure models for each phase in the clinker. From these data one can obtain pattern intensity information that may be related to phase abundance. Additional data on the chemical and structural properties of each phase may also be obtained. This approach to processing XRD data can be used in research and for quality control in cement production, and is used here to analyze the NIST Reference Clinkers. This method is acceptable under ASTM C 1365, where users are required to qualify their instruments and procedures. Initial crystal structure models were taken from the literature [7-11, 14] and are provided in Appendix A.

Experimental Methods

Sample preparation

A representative sampling of each clinker was obtained through use of a random-stratified sampling scheme and totaled nine samples. Each of these samples was split into replicates designated a and b for a total of 18 specimens. Each replicate was analyzed twice, so for all three clinkers there were 54 samples and 108 scans. The specimen analysis sequencing was randomized so as to avoid confounding with any effects of machine drift. For example, RM 8486 sample 1, replicates a and b, were analyzed during scans 12, 46, 32, and 65.

The clinkers are millimeter-sized fragments to provide a relatively homogeneous material, yet be suitable for microscopic analysis. Particle size requirements for XRD necessitate reduction in particle

size to below 10 μm to maximize the number of particles analyzed, improve powder homogeneity and packing characteristics, and minimize microabsorption-related problems.

Each vial of clinker (about 10 g) was split into replicates using the cone-and-quarter technique for subsampling a material. The clinker is poured onto a weighing paper and the mound is then divided into quarters using a small spatula. Opposite quarters are combined as equal splits of the original sample. The splits were ground individually to fineness less than about 250 μm using a mortar and pestle. Final grinding employed a micronizing mill[1,2] to reduce the clinker to a mean particle size of about 2 μm in 10 min, using 200-proof ethanol (about 5 ml) as a grinding lubricant. The median particle size estimate is based upon a single measurement using an X-Ray absorption particle settling system. The ground clinker was vacuum filtered to remove the ethanol, dried at 60 °C, and then placed in a sealed vial over desiccant in a vacuum dissector.

Analysis

Data were collected using Cu Kα radiation from 2Θ = 18° to 130°, using a step size of 0.02°, a count time of 4 s, and a graphite monochromator. The receiving slit was fixed at 0.2 mm and a fixed divergence slit approximately 0.9° to satisfied the requirement for a constant irradiated volume as GSAS calculates diffraction patterns on a fixed slit basis.

The first step was to establish suitable experiment files for the crystal structures and peak shapes for the phases in each clinker by analyzing chemical extraction residues. Structure models from the literature (Figure 1 and Table 1, Appendix A), were used for the refinement. This simplified subsequent analyses by allowing refinement of each structure model and the peak shape parameters with less interference from the other constituents. These intermediate models and peak shapes were used for the analyses of the bulk clinker patterns. In essence, the bulk clinker analyses are pattern-fitting exercises using reference standards determined from the extraction residue experiments. The potassium hydroxide/sucrose extraction (KOSH) concentrates the silicate fraction, the salicyclic acid/methanol extraction (SAX) concentrates the interstitial phases, and a 7 %, by volume, nitric acid in methanol extraction provides a ferrite and periclase residue [12]. A description of these procedures is provided in Appendix B.

Variables refined for each phase include scale, specimen displacement, background, lattice parameters, atomic coordinates (subject to Si-O or Ca-O bond length constraints), aluminum and iron fractions in ferrite tetrahedral and octahedral sites, peak shapes, and, for alite, preferred orientation. Fixing these variables, especially the profile shape parameters, in the subsequent analyses eliminated problematic correlations.

[1] Certain products are identified to more fully describe the analytical procedure. In no case does this imply endorsement by the National Institute of Standards and Technology, nor does it mean that they are the best available for the purpose.
[2] McCrone micronizing mill, McCrone Research, Chicago, Illinois.

Phase: β-Dicalcium Silicate **Formula:** Ca_2SiO_4 **ICDD:** 33-302 (larnite)

Reference: K.H. Jost, B. Ziemer and R. Seydel "Redetermination of the Structure of β-Dicalcium Silicate," *Acta Cryst*. (1977). **B33**, 1696-1700

Symmetry: Monoclinic $P2_1/n$ **Z:** 4 **Mass, Formula Unit:** 3.326 g cm^{-3}

Cell Parameters (Å)
a 5.502 **b** 6.745 **c** 9.297 **β** = 94.59° **Vol (Å^3):** 343.9

Atomic Parameters

	x	y	z	B (Å^2)
Ca(1)	0.2738	0.3428	0.5694	0.38
Ca(2)	0.2798	0.9976	0.2981	0.30
Si	0.2324	0.7841	0.5817	0.19
O(1)	0.2864	0.0135	0.5599	0.91
O(2)	0.0202	0.7492	0.6919	0.67
O(3)	0.4859	0.6682	0.6381	0.63
O(4)	0.1558	0.6710	0.4264	0.62

Average interatomic distances
Si - O: 1.63 Å , **Ca - O**: 2.88 Å

Typical bulk belite composition (from Taylor '90, Cement Chemistry)

Na_2O	MgO	Al_2O_3	SiO_2	P_2O_5	SO_3	K_2O	CaO	TiO_2	Mn_2O_3	Fe_2O_3
0.1	0.5	2.1	31.5	0.2	0.1	0.9	63.5	0.2	0.0	0.9

This reference: $(K_{0.01}\ Na_{0.005}\ Ca_{0.975}\ Mg_{0.01})_2\ (Fe_{0.02}\ Al_{0.06}\ Si_{0.90}\ P_{0.01}\ S_{0.01})O_{3.96}$

Figure 4: Crystal structure database entry for belite (β-form).

Microabsorption Corrections

Microabsorption results in biased phase fraction estimates. The greater the individual phases linear attenuation coefficient from that of the mixture, the greater the error of the phase fraction estimate. Weakly-absorbing phases exhibit greater intensities than expected, while strongly absorbing phases exhibit lower intensities. Calculation of the linear attenuation coefficients for the cement phases (Table 1) and for a mixture, RM 8486, shows that ferrite, periclase, and free lime (when present) may be expected to have the greatest error unless compensated for. This effect is not problematic in studies utilizing standardization mixtures, as the error is inherent in the standardization curve; however, in Rietveld analyses this effect may be significant.

Microabsorption effects are reduced through fine grinding, but trials using binary mixtures of ferrite and periclase show they may still be problematic. Use of the Brindley absorption correction changes the scale factors based upon the differences between the phase and mixture linear attenuation coefficients, with an adjustment made for particle size [13]. Using the actual median particle size of 2μm resulted in an over correction of the phase fractions of the known mixture. An example showing true values versus raw data and Brindley-corrected values based upon a 1μm median particle size, is provided in Figure 5. As expected, ferrite and periclase values better reflect the true values based upon the laboratory-prepared mixture. The low value for orthorhombic aluminate may partly result from impurities in the laboratory material.

Table 1: Linear Attenuation Coefficients (μ) (for Cu Kα radiation)

Phase	Composition	μ	μ / μ clinker
Alite	Ca_3SiO_5	308	1.0
Belite	Ca_2SiO_4	294	1.0
Aluminate	$Ca_3AL_2O_6$	260	0.9
C4AF	$Ca_2(Al,Fe)_2O_5$	496	1.7
Free Lime	CaO	398	1.4
Periclase	MgO	100	0.3
Arcanite	K_2SO_4	226	0.8
RM 8486	Bulk Clinker	290	1.0

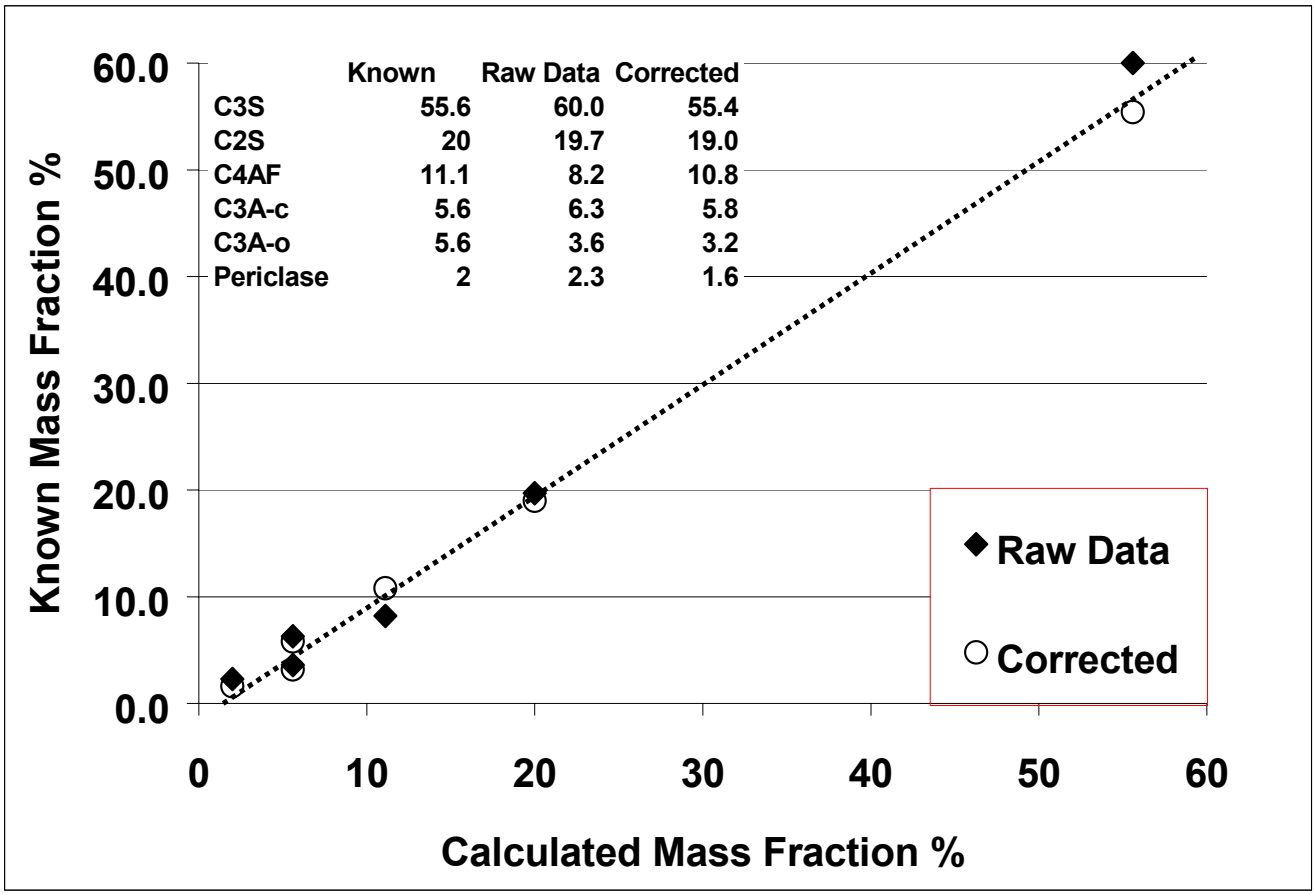

Figure 5: True versus calculated mass fraction values for a laboratory-prepared mixture of clinker phases showing both raw data (diamonds) and data corrected for microabsorption (circles) using the Brindley microabsorption correction and a median particle size of 1 μm.

Data Presentation and Evaluation

Figure 5 shows a composite plot of the raw data, the calculated peak locations for each phase (tic marks at base of plot), the calculated pattern (green trace), and difference plot. Graphical comparison of the observed versus the calculated pattern, residual plots, the normalized error distribution and normal probability plots of the residuals (Figure 6) are perhaps the best means by which to judge the quality of the fit. For the normal probability plot of the normalized residuals, a linear plot with a zero intercept and unit slope indicates that the error is normally distributed. Numerical assessment of the fit is made using a chi-squared value, with lower values reflecting an improved fit. The refinement was stopped when the fit could not be significantly improved.

Quantitative Analysis

Simultaneous refinement of X-ray diffraction patterns of multiple phases allows quantitative analysis using equation 1, whose variables (aside from Z) are all refined in the fitting process:

$$W_p = (S_p (ZMV)_p) / (\Sigma [S (ZMV)]) \quad (1)$$

where

- W_p = the mass fraction of phase p,
- S = the Rietveld scale factor,
- Z = the number of formula units per unit cell,
- M = the mass of the formula unit, and
- V = the unit cell volume.

Initial estimates of the phase fractions were used to estimate the linear absorption coefficient of the mixture. A second quantitative estimate using a Brindley absorption correction, based upon a mean particle size of 1 μm, established the final analyses. Phase abundance estimates of polymorphs of specific phases, such as β-C_2S and α-C_2S or cubic and orthorhombic C_3A were summed for comparison with the optical microscopy data.

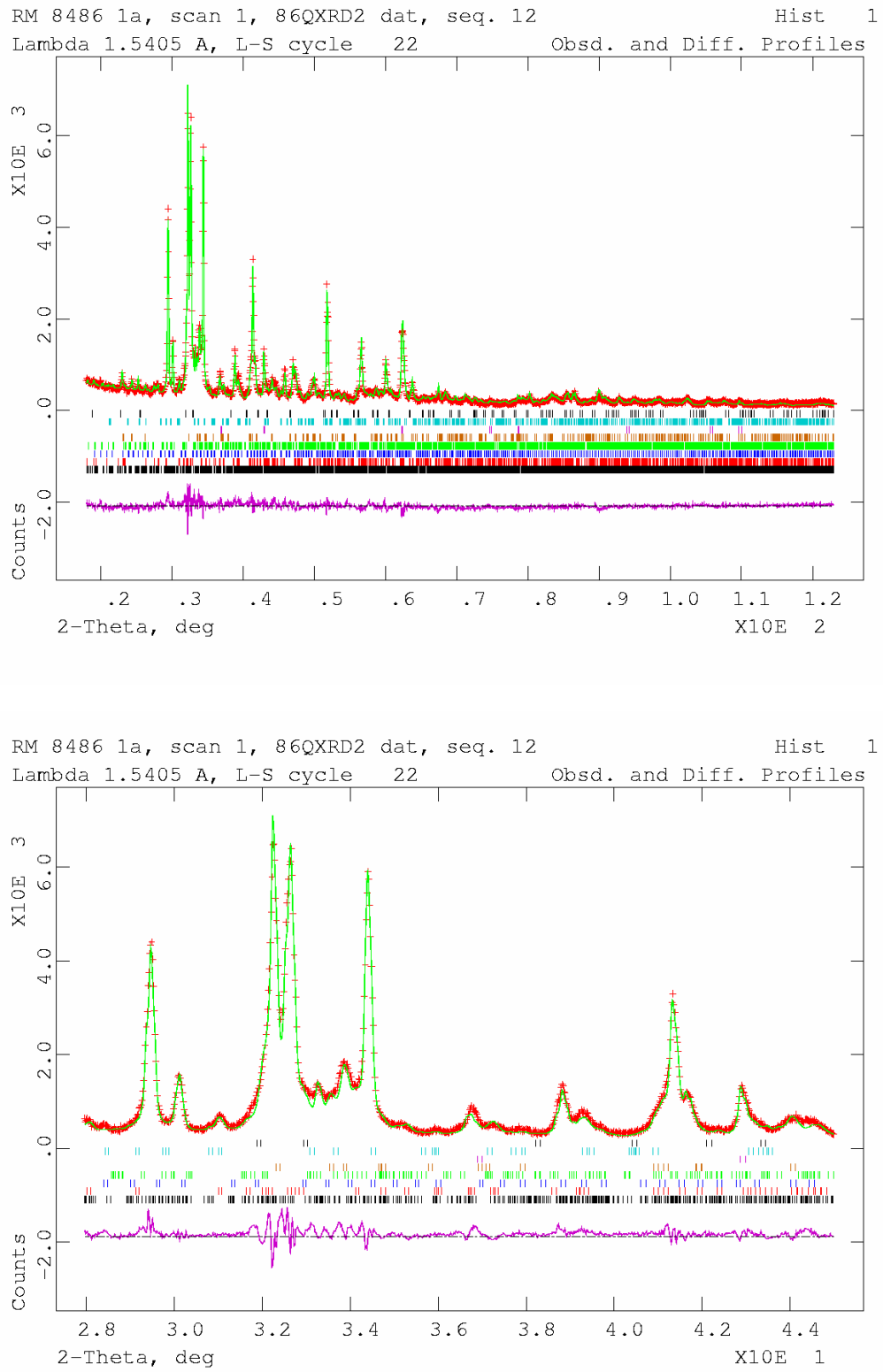

Figure 6. Refined data for sample 1a showing raw, best-fit, and difference curves. The tic marks show peak positions for (bottom up) alite, belite (β and α forms), ferrite, cubic and orthorhombic aluminates, and periclase.

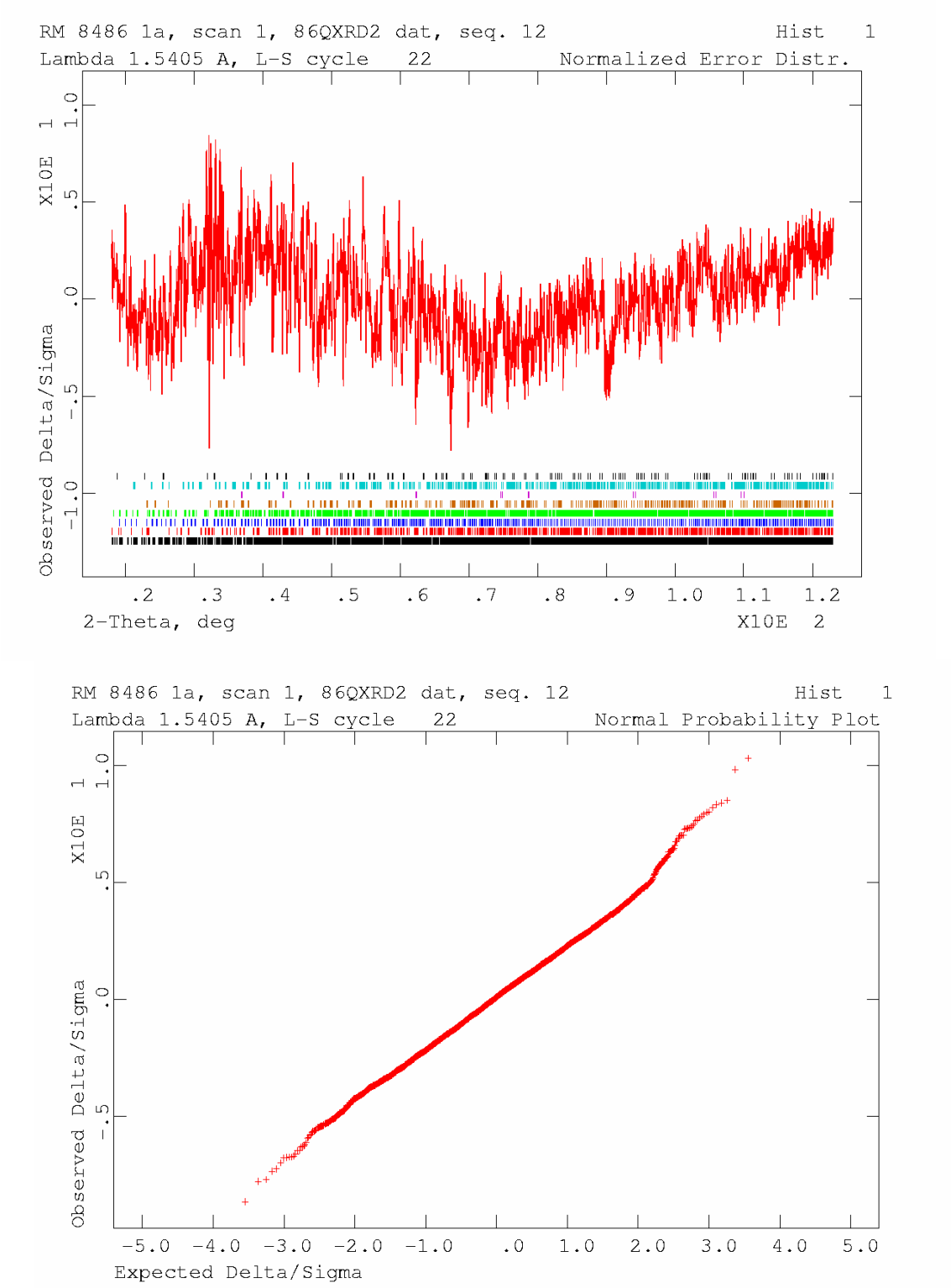

Figure 7. A straight normal probability plot of the errors indicates their distribution is well approximated by a Gaussian.

Table 2. RM 2686 mass fraction (percent) by QXRD, optical data (OM), and round robin data (RR) following ASTM C 1356 [2]. QXRD analysis of nine vials (1-9) with two splits per vial (a, b), with each split analyzed in duplicate (1, 2).

	Alite	Belite	Ferrite	Aluminate	Periclase
1a1	**56.4**	**21.5**	**13.8**	**3.9**	**4.3**
1a2	**56.8**	**21.8**	**14.0**	**3.3**	**4.0**
1b1	**55.1**	**21.1**	**16.1**	**3.6**	**4.2**
1b2	**56.1**	**20.3**	**15.7**	**3.7**	**4.3**
2a1	**56.8**	**20.9**	**14.6**	**3.5**	**4.2**
2a2	**56.5**	**21.7**	**14.4**	**3.4**	**4.0**
2b1	**58.5**	**20.8**	**13.9**	**3.1**	**3.7**
2b2	**58.5**	**21.0**	**13.5**	**3.2**	**3.8**
3a1	**56.8**	**21.5**	**14.2**	**3.3**	**4.2**
3a2	**57.0**	**21.2**	**14.5**	**3.4**	**3.9**
3b1	**58.6**	**20.4**	**13.7**	**3.3**	**3.9**
3b2	**57.4**	**20.6**	**14.5**	**3.5**	**4.1**
4a1	**56.3**	**21.1**	**15.0**	**3.4**	**4.2**
4a2	**56.2**	**21.5**	**14.9**	**3.3**	**4.1**
4b1	**56.7**	**20.9**	**14.8**	**3.5**	**4.1**
4b2	**56.9**	**20.9**	**14.7**	**3.5**	**4.1**
5a1	**55.8**	**20.6**	**15.7**	**3.5**	**4.4**
5a2	**55.7**	**20.8**	**15.8**	**3.5**	**4.2**
5b1	**57.2**	**21.1**	**14.1**	**3.4**	**4.2**
5b2	**57.1**	**21.0**	**14.1**	**3.4**	**4.3**
6a1	**56.9**	**21.5**	**14.1**	**3.4**	**4.0**
6a2	**56.8**	**21.4**	**14.1**	**3.4**	**4.3**
6b1	**57.3**	**20.7**	**14.2**	**3.6**	**4.2**
6b2	**57.0**	**20.5**	**15.0**	**3.5**	**3.9**
7a1	**55.9**	**21.4**	**14.9**	**3.5**	**4.3**
7a2	**56.5**	**20.7**	**14.8**	**3.5**	**4.6**
7b1	**56.5**	**21.5**	**14.3**	**3.4**	**4.3**
7b2	**56.9**	**21.1**	**14.2**	**3.6**	**4.1**
8a1	**56.7**	**21.2**	**14.4**	**3.5**	**4.2**
8a2	**57.0**	**21.1**	**14.3**	**3.5**	**4.0**
8b1	**56.9**	**20.6**	**15.0**	**3.4**	**4.1**
8b2	**56.3**	**21.1**	**14.8**	**3.5**	**4.2**
9a1	**55.8**	**21.4**	**15.1**	**3.5**	**4.3**
9a2	**56.9**	**20.8**	**14.6**	**3.5**	**4.2**
9b1	**56.1**	**21.0**	**15.3**	**3.5**	**4.1**
9b2	**57.2**	**20.8**	**14.8**	**3.4**	**3.8**
OM1 a	**59.0**	**23.0**	**13.0**	**1.1**	**3.0**
OM1 b	**56.3**	**25.3**	**13.1**	**1.1**	**3.7**
OM1 c	**60.3**	**20.6**	**14.2**	**1.0**	**3.7**
OM1 d	**58.1**	**23.7**	**14.1**	**1.0**	**3.7**
RR1 a	**56.8**	**23.6**	**13.5**	**3.2**	**1.9**
RR1 b	**56.2**	**24.1**	**14.3**	**2.5**	**2.0**
RR2 a	**60.0**	**23.6**	**9.6**	**1.3**	**4.7**
RR2 b	**60.2**	**24.6**	**8.1**	**2.3**	**3.8**
RR3 a	**61.8**	**23.9**			**2.5**
RR3 b	**60.6**	**25.0**			**2.8**

Table 3. RM 2687 mass fraction (percent) by QXRD, optical data (OM), and round robin data (RR) following ASTM C 1356 [2]. QXRD analysis of nine vials (1-9) with two splits per vial (a, b), with each split analyzed in duplicate (1, 2).

	Alite	Belite	Ferrite	Aluminate	Arcanite	Free Lime*
1a1	74.7	11.2	4.3	8.3	0.6	
1a2	74.2	11.2	4.7	8.5	0.6	
1b1	74.3	11.5	4.3	8.3	0.7	
1b2	74.4	11.7	4.3	8.1	0.6	
2a1	74.4	11.6	4.3	8.3	0.6	
2a2	74.2	11.8	4.3	8.3	0.6	
2b1	74.6	11.5	4.4	8.0	0.6	
2b2	74.2	11.6	4.3	8.3	0.7	
3a1	74.4	11.4	4.4	8.3	0.6	
3a2	74.4	11.4	4.4	8.3	0.5	
3b1	74.2	11.4	4.6	8.2	0.6	
3b2	73.5	11.4	4.5	9.1	0.6	
4a1	74.5	11.1	4.5	8.4	0.6	
4a2	73.8	11.4	4.8	8.3	0.6	
4b1	73.8	11.4	4.8	8.3	0.6	
4b2	73.6	11.6	4.7	8.4	0.6	
5a1	73.8	11.4	4.8	8.5	0.6	
5a2	73.8	11.5	4.7	8.5	0.6	
5b1	74.2	11.9	4.2	8.1	0.6	
5b2	74.4	11.8	4.3	8.0	0.6	
6a1	74.1	11.6	4.4	8.3	0.6	
6a2	74.0	11.4	4.8	8.3	0.6	
6b1	74.2	11.6	4.5	8.3	0.5	
6b2	74.5	11.4	4.4	8.3	0.5	
7a1	74.2	11.2	4.5	8.6	0.6	
7a2	74.7	10.8	4.5	8.5	0.6	
7b1	74.7	11.3	4.2	8.4	0.6	
7b2	74.9	11.0	4.3	8.4	0.5	
8a1	73.9	11.3	4.9	8.5	0.5	
8a2	74.3	11.2	4.7	8.4	0.6	
8b1	74.1	11.2	4.6	8.6	0.6	
8b2	73.7	11.7	4.7	8.3	0.6	
9a1	73.8	11.5	4.7	8.4	0.6	
9a2	74.0	11.6	4.5	8.3	0.6	
9b1	74.0	11.9	4.3	8.3	0.7	
9b2	74.1	11.5	4.6	8.3	0.6	
OM1 a	73.19	7.29	4.00	12.43	0.82	2.25
OM1 b	71.64	9.59	3.72	12.29	0.62	1.91
OM1 c	73.25	7.14	2.78	12.82	0.98	3.01
OM1 d	75.46	6.98	2.56	10.82	1.49	2.63
RR1 a	72.24	9.10	1.46	13.23	1.69	2.24
RR1 b	72.51	9.79	0.88	13.32	1.48	1.99
RR2 a	70.42	9.00	0.92	15.63	0.00	4.03
RR2 b	71.92	8.50	1.20	14.50	0.00	3.88
RR3 a	76.93	8.31	1.00	13.40	0.00	1.86
RR3 b	76.11	8.29	1.00	10.40	0.00	1.57

* XRD data did not measure free lime as it was altered during sample preparation and storage.

Table 4. RM 2688 mass fraction (percent) by QXRD, optical data (OM), and round robin data (RR) following ASTM C 1356 [2]. QXRD analysis of nine vials (1-9) with two splits per vial (a, b), with each split analyzed in duplicate (1, 2).

	Alite	Belite	Ferrite	Aluminate
1a1	**67.2**	**14.8**	**14.3**	**3.7**
1a2	**68.2**	**13.9**	**14.3**	**3.7**
1b1	**67.5**	**14.1**	**14.8**	**3.6**
1b2	**66.9**	**14.7**	**14.7**	**3.7**
2a1	**66.7**	**14.9**	**14.8**	**3.6**
2a2	**67.3**	**14.0**	**14.9**	**3.7**
2b1	**67.0**	**15.0**	**14.3**	**3.8**
2b2	**67.1**	**15.5**	**13.7**	**3.7**
3a1	**65.8**	**15.2**	**15.1**	**3.8**
3a2	**66.7**	**14.8**	**14.6**	**3.9**
3b1	**67.3**	**14.0**	**14.8**	**3.8**
3b2	**67.5**	**14.1**	**14.6**	**3.8**
4a1	**68.0**	**13.7**	**14.6**	**3.7**
4a2	**68.0**	**14.1**	**14.5**	**3.5**
4b1	**67.3**	**14.8**	**14.2**	**3.6**
4b2	**67.3**	**14.9**	**14.2**	**3.6**
5a1	**66.6**	**15.6**	**14.1**	**3.7**
5a2	**67.4**	**14.5**	**14.3**	**3.9**
5b1	**67.4**	**14.8**	**14.2**	**3.7**
5b2	**67.4**	**14.8**	**14.0**	**3.7**
6a1	**66.1**	**15.4**	**14.7**	**3.8**
6a2	**66.5**	**14.7**	**14.8**	**4.0**
6b1	**66.9**	**15.2**	**14.3**	**3.7**
6b2	**67.4**	**15.0**	**14.0**	**3.6**
7a1	**68.2**	**14.6**	**13.5**	**3.7**
7a2	**68.3**	**14.5**	**13.6**	**3.6**
7b1	**67.5**	**15.1**	**13.9**	**3.5**
7b2	**68.0**	**14.7**	**13.9**	**3.5**
8a1	**67.3**	**14.4**	**14.5**	**3.9**
8a2	**68.0**	**13.9**	**14.3**	**3.7**
8b1	**68.7**	**15.2**	**12.7**	**3.4**
8b2	**69.1**	**15.3**	**12.2**	**3.4**
9a1	**69.0**	**16.0**	**11.7**	**3.4**
9a2	**68.9**	**15.4**	**12.3**	**3.4**
9b1	**68.1**	**15.8**	**12.6**	**3.5**
9b2	**69.2**	**14.5**	**12.7**	**3.6**
OM1 a	**65.14**	**18.30**	**13.46**	**3.08**
OM1 b	**64.98**	**19.31**	**11.56**	**4.15**
OM1 c	**64.20**	**18.48**	**13.20**	**3.87**
OM1 d	**65.54**	**17.94**	**10.25**	**6.24**
RR1 a	**63.40**	**19.82**	**12.77**	**4.02**
RR1 b	**64.06**	**19.37**	**12.03**	**4.53**
RR2 a	**65.52**	**19.92**	**7.80**	**6.76**
RR2 b	**67.72**	**17.21**	**7.54**	**7.54**
RR3 a	**67.35**	**18.09**	**9.80**	**4.80**
RR3 b	**67.82**	**18.16**	**8.20**	**8.20**

Table 5. RM Clinker QXRD Summary: 95 % Confidence Limits for the Mean (Mass Percent).

Limits	Lower	Mean	Upper
RM 8486			
Alite	**56.50**	**56.75**	**57.00**
Belite	**20.91**	**21.04**	**21.17**
Aluminate	**3.41**	**3.46**	**3.50**
Ferrite	**14.40**	**14.61**	**14.81**
Periclase	**4.07**	**4.13**	**4.20**

Limits	Lower	Mean	Upper
RM 8487			
Alite	**73.51**	**74.18**	**74.85**
Belite	**10.95**	**11.44**	**11.92**
Aluminate	**7.98**	**8.35**	**8.73**
Ferrite	**4.11**	**4.51**	**4.91**
Periclase	**0.77**	**0.91**	**1.05**

Limits	Lower	Mean	Upper
RM 8488			
Alite	**65.91**	**67.55**	**69.18**
Belite	**13.64**	**14.77**	**15.90**
Aluminate	**3.36**	**3.66**	**3.96**
Ferrite	**12.33**	**14.02**	**15.71**

Graphical Analyses: Box Plots

The box plot is a schematic graphical device for comparing the empirical distributions represented by batches of numbers [15]. For these data, the analytical method used (QXRD, OM-1, RR1-n) identifies the batches. This plot can be considered a visual one-way analysis of variance (anova) or t-test. The location of the distributions, their spread, and extremes are embedded in the graphical display. This allows meaningful comparison of distributional information through rapid assessment of the alignment or misalignment of median values and boxes, and differences in spread.

Important features of the box plot are:

1. the width of the box is proportional to sample size,
2. the median value, used as an indicator of location because of its resistance to outliers, is identified by the X,
3. the interquartile range ("middle half") of the data are represented by the body of the box, and
4. the extremes (minimum and maximum) are represented by the ends of the straight lines projecting out of the box.

One important consideration for these data are that the QXRD box represents 36 numbers, while the RM certificate data (OM) represents only four numbers, and the round robin data (RR) represents just two numbers each. The boxes for the RR groups, with only two observations, have the upper line of the box equal to one data point, the other line equal to the other, and the X in the middle denoting the mean/median of the two observations.

Direct Phase Estimates by Microscopy and QXRD

Both microscopical and QXRD methods have been used to estimate phase abundance of clinker and are considered direct methods of analysis. Error in microscopy due to incorrect identification of the constituent phases is considered to exceed the error due to counting statistics [15] as fineness of the constituents may preclude their identification. For the finer-grained clinkers this may be especially problematic for periclase, free lime, and the alkali sulfates.

X-ray powder diffraction analyses are not limited by crystal size and so are suitable for both clinker and cements. The accuracy of XRD, given careful experimental procedure, is about 2 % to 5 % absolute for alite and belite and 1 % to 2 % for aluminate and ferrite [15]. Grinding to a particle size of a few micrometers is a necessary preparation step and a consequence is the improved homogeneity of a relatively coarse-grained material, and resulting improved data precision. Generally, one should see good agreement between XRD and microscopy for the silicates and the total interstitial phases.

Limitations of the accuracy derive from the suitability of the reference standards (the structure models), and the ability to identify and control correlations between variables. For example, because of a high degree of overlap of the strong diffraction peaks from cubic and orthorhombic aluminate, their scale (intensity) factors are correlated. These correlations can be controlled through determination of the peak profile shape characteristics using a salicylic acid / methanol extraction residue enriched in aluminate. In fitting the whole-clinker pattern, these profile shape variables served as initial values and, for both aluminate forms, were constrained to be the same. Box plots of the initial data set showed an anti-correlation between belite and ferrite. In this case, the peak shape of ferrite would broaden at the expense of the intensity factor of belite. This was controlled by determining their respective peak profile shape parameters using potassium hydroxide / sucrose and nitric acid / methanol extraction residues and holding the shape parameters fixed throughout the fitting of the whole-clinker patterns.

RM 8486

RM 8486 exhibits an intermediate crystal size and high heterogeneity relative to the other clinkers that may result in greater spread in the phase fraction estimates (Figure 7). Alite (Figure 8) shows reasonable similarity between XRD, OM-1 and RR-1, with RR-2 and RR-3 being higher. OM-1 with its 4 points has significantly greater spread (IQ-range) than the more tightly grouped XRD numbers. For belite (Figure 9), the optical points diverge from the XRD yet demonstrate reasonable agreement along themselves, although OM-1 again displays large variance, with only the lowest point comparing favorably with XRD.

Aluminate values (Figure 10) do not demonstrate good agreement among XRD and optical data. Here OM-1 appears to be a lowlier. This may result from the fine crystal size and resulting difficulty in seeing this phase. Ferrite estimates (Figure 11) exhibit reasonable agreement among XRD, OM-1, and RR-1, both in terms of level (mean/median) and spread. Periclase estimates (Figure 12) fall into two groupings with respect to the mean/median: XRD/OM/RR-2 versus RR-1/RR-3.

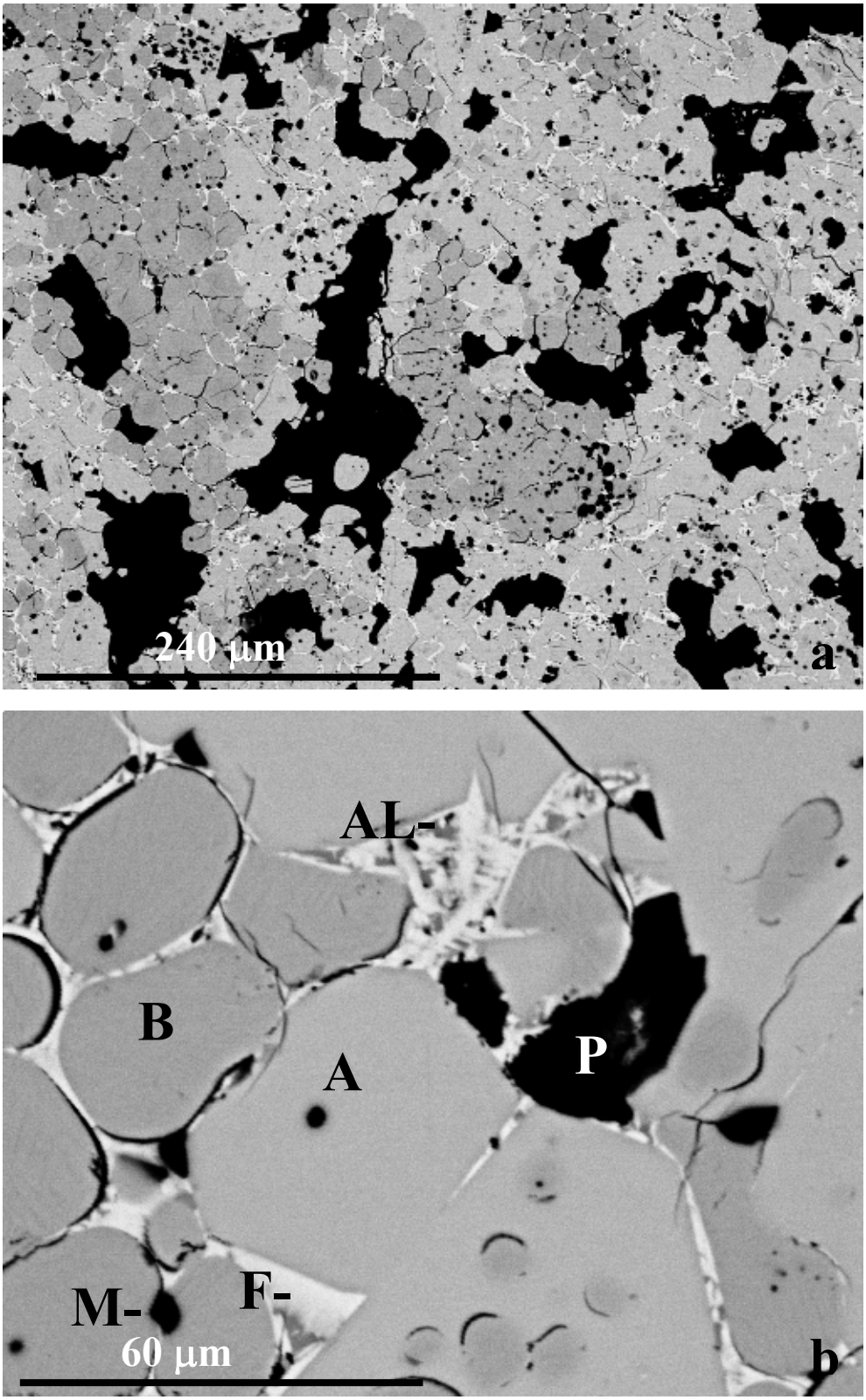

Figure 8. Backscattered electron SEM images of RM 8486 at low (a) and high (b) magnifications show the heterogeneous texture and intermediate crystal size with alite (A), belite (B), ferrite (F), aluminate (AL), periclase (M), and pores (P).

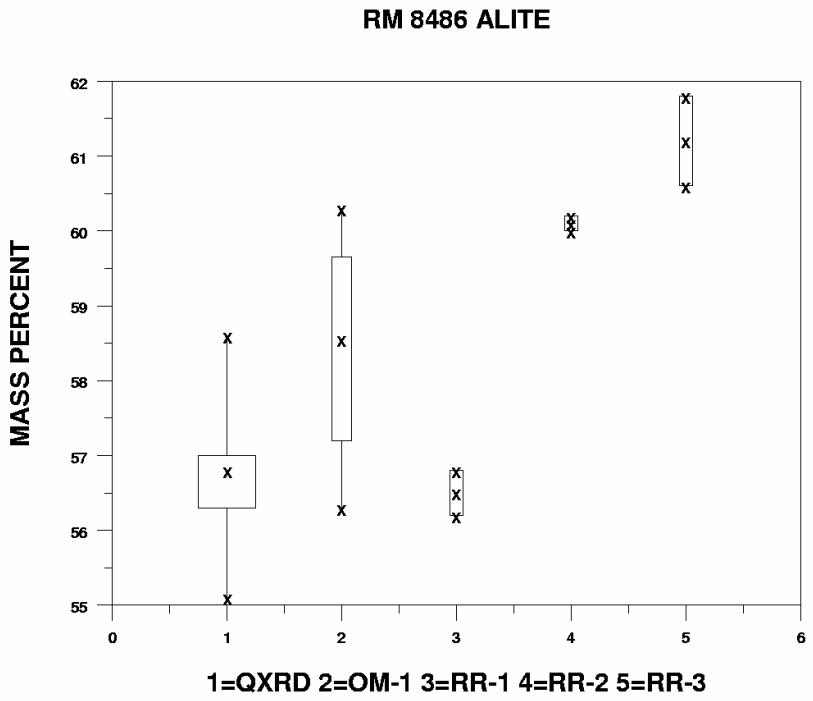

Figure 9. Box plot for RM 8486 alite phase estimates by QXRD, optical microscopy (OM), and round robin (RR).

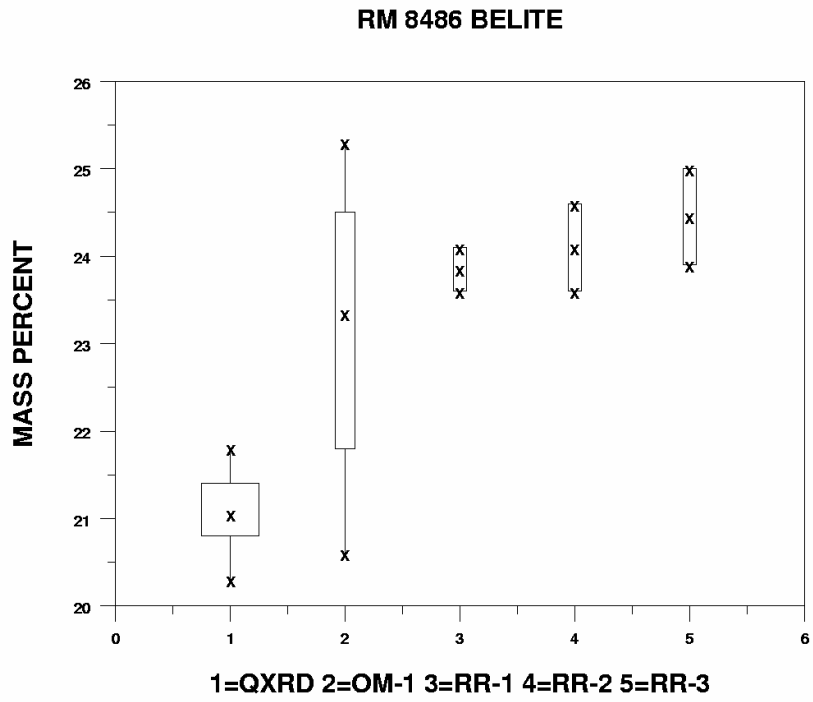

Figure 10. Box plot for RM 8486 Belite.

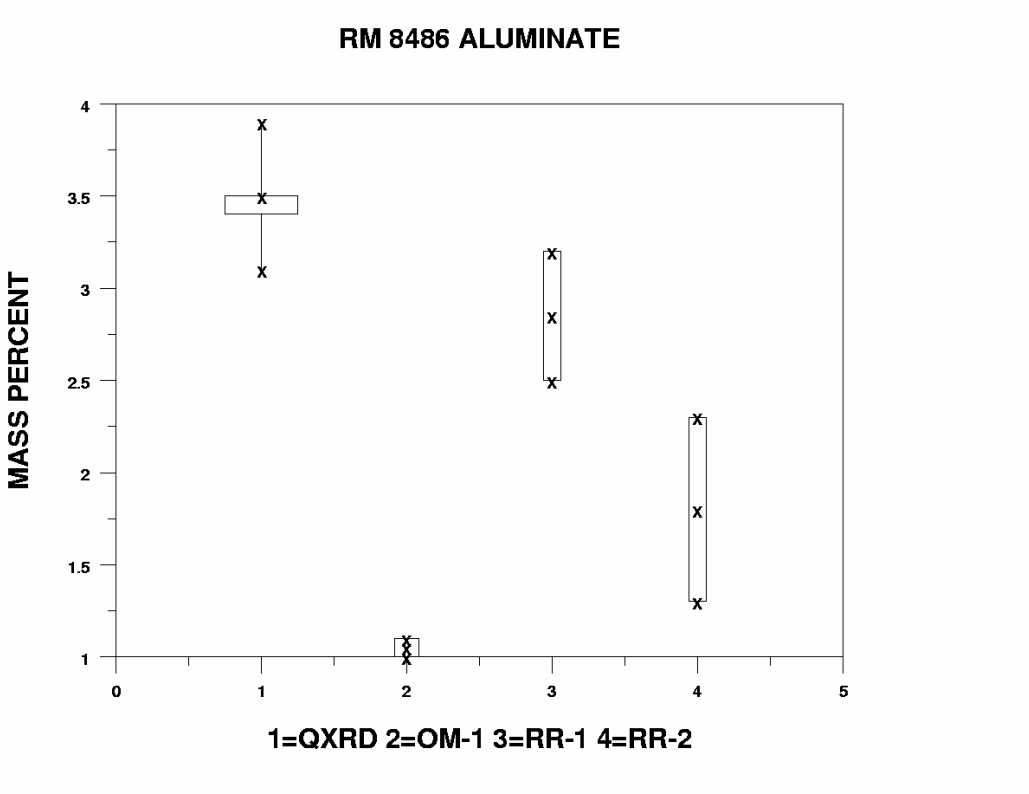

Figure 11. Box plot for RM 8486 aluminate

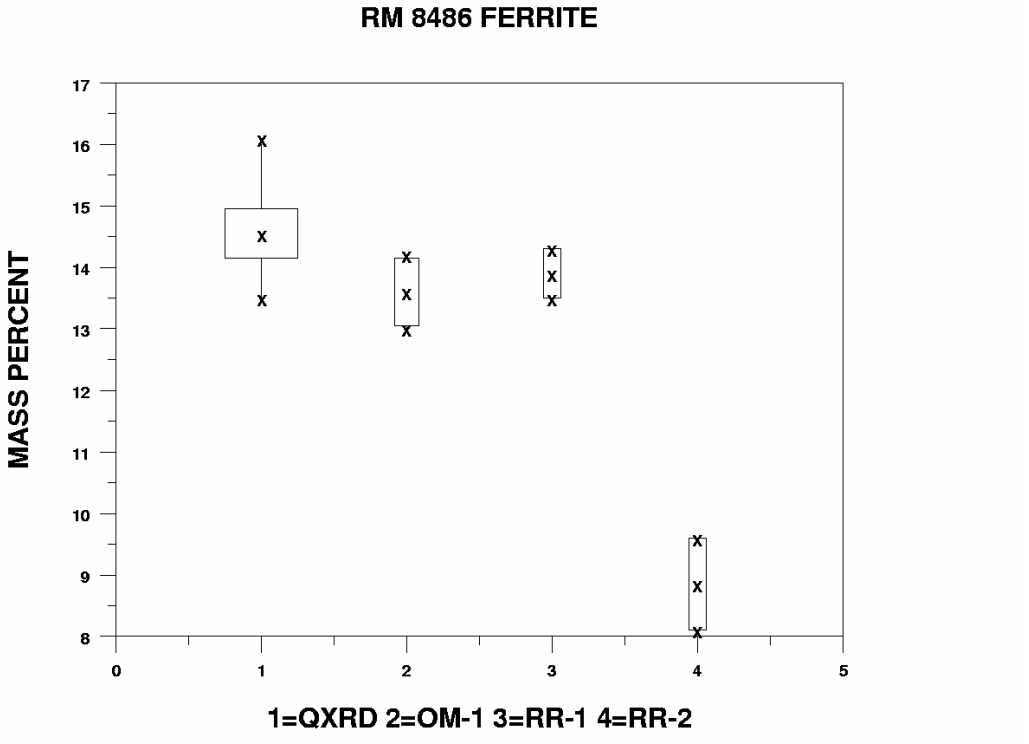

Figure 12. Box plot for RM 8486 ferrite.

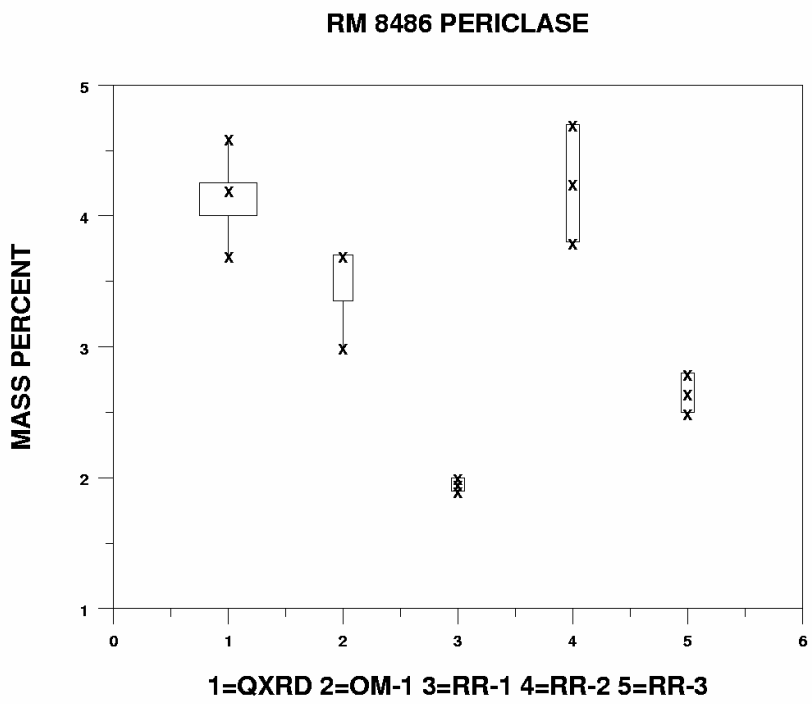

Figure 13. Box plot for RM 8486 periclase.

RM 8487

RM 8487, being the finest-grained of the three clinkers, was expected to be the most difficult to analyze using microscopy. Typical microstructures showing a heterogeneous distribution of the silicates (alite and belite), may result in the greater uncertainties observed in the optical analyses. The ferrite phase ranged from fine-grained to extremely fine- grained and may in some cases be difficult to distinguish visually from the aluminate. A backscattered electron scanning electron microscope image of the interstitial phases (Figure 13) shows the finely-intermixed aluminate and ferrite. This microstructure probably would not be recognized using optical microscopy. The fine-grained distribution does not pose difficulties for the X-ray analyses.

Alite (Figure 14) shows reasonable similarity between XRD, OM-1 and RR-1, with RR-2 and RR-3 being somewhat lower and higher, respectively. OM-1 with its 4 points has significantly greater spread (IQ-range) than the more tightly grouped XRD numbers. For belite (Figure 15), the optical points diverge from the XRD yet demonstrate reasonable agreement between themselves, although OM-1 again displays large variance.

Aluminate values (Figure 16) do not demonstrate good agreement between XRD and optical data, with XRD values lower than the optical data. Ferrite values show a reverse trend (Figure 17), with XRD values slightly higher than optical. These findings may result from the fine crystal size which made it difficult to see this phase using the optical microscope. Alkali sulfate was identified by optical microscopy and was identified in the bulk XRD patterns as arcanite. The XRD and OM-1 data show reasonable agreement.

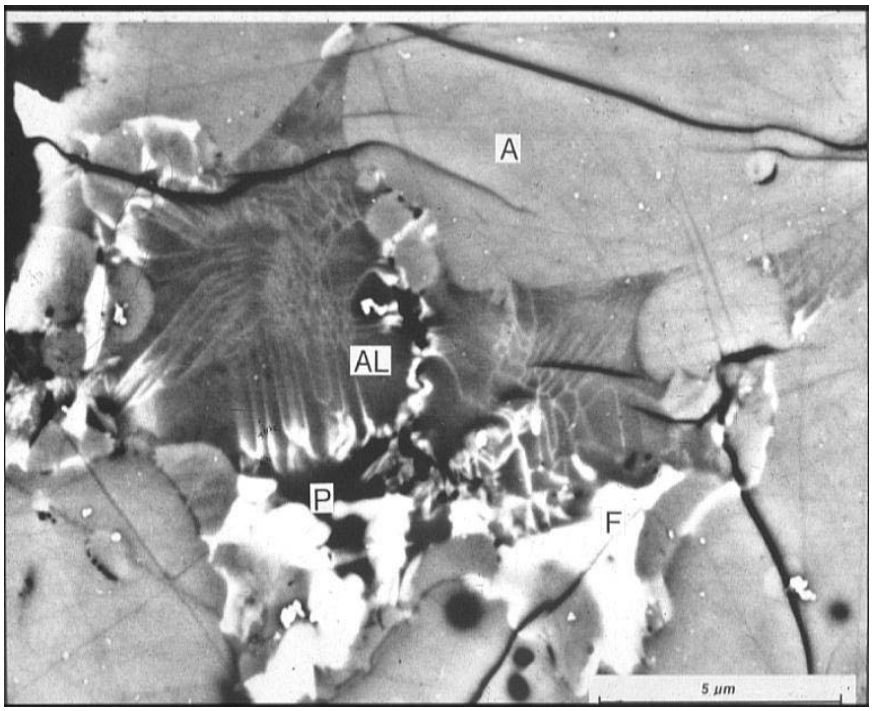

Figure 14. SEM backscattered electron image of the interstitial phase of RM 8487 shows the intermixing of ferrite (F, bright phase) and aluminate (AL, dark) not observable by optical microscopy. Other phases shown here are alite (A), and porosity (P).

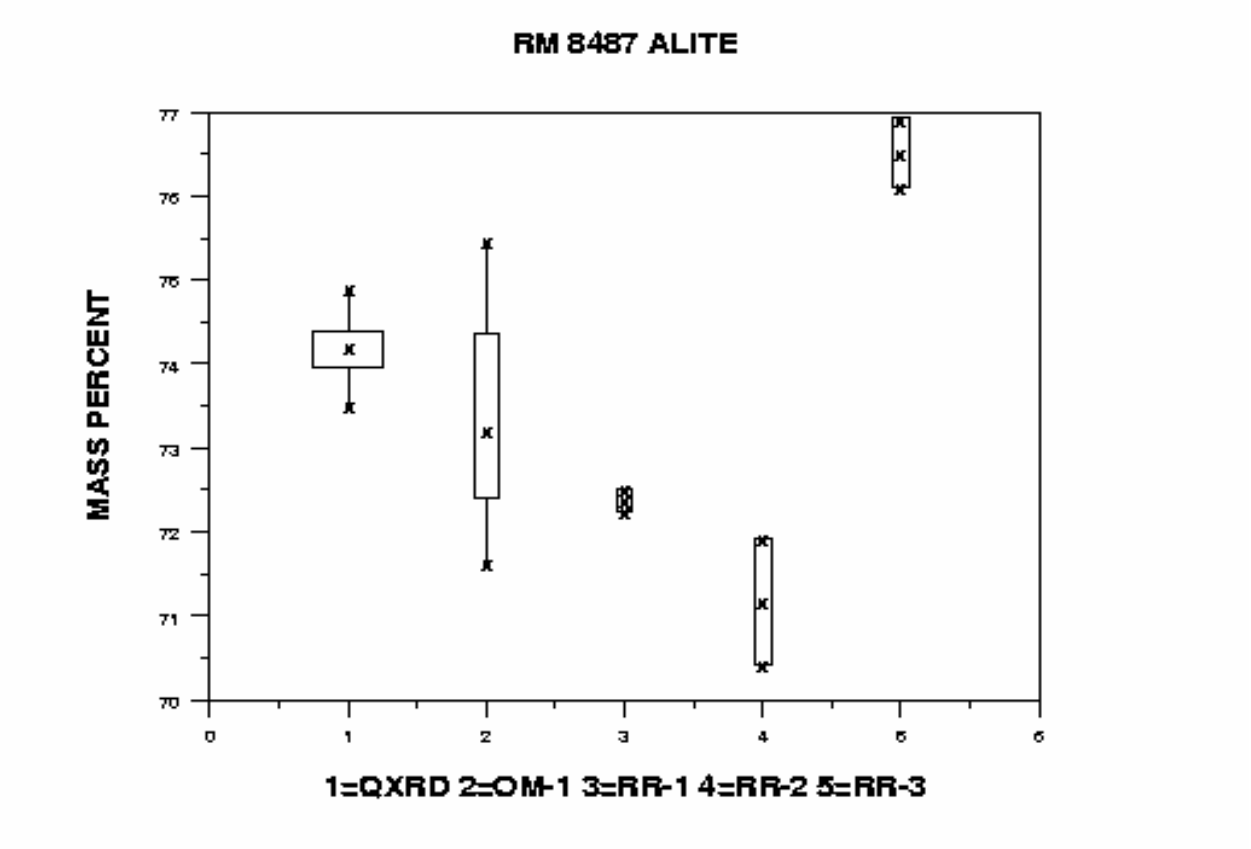

Figure 15. Box plot for RM 8487 alite.

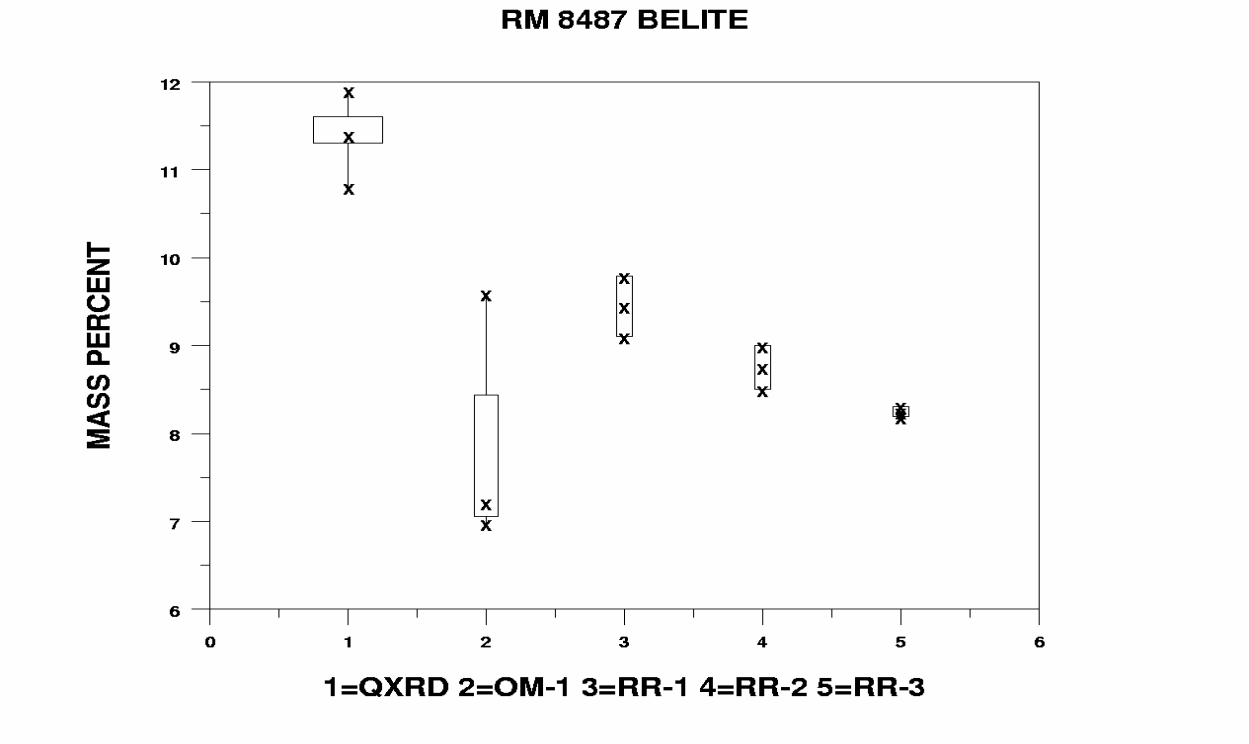

Figure 16. Box plot for RM 8487 belite.

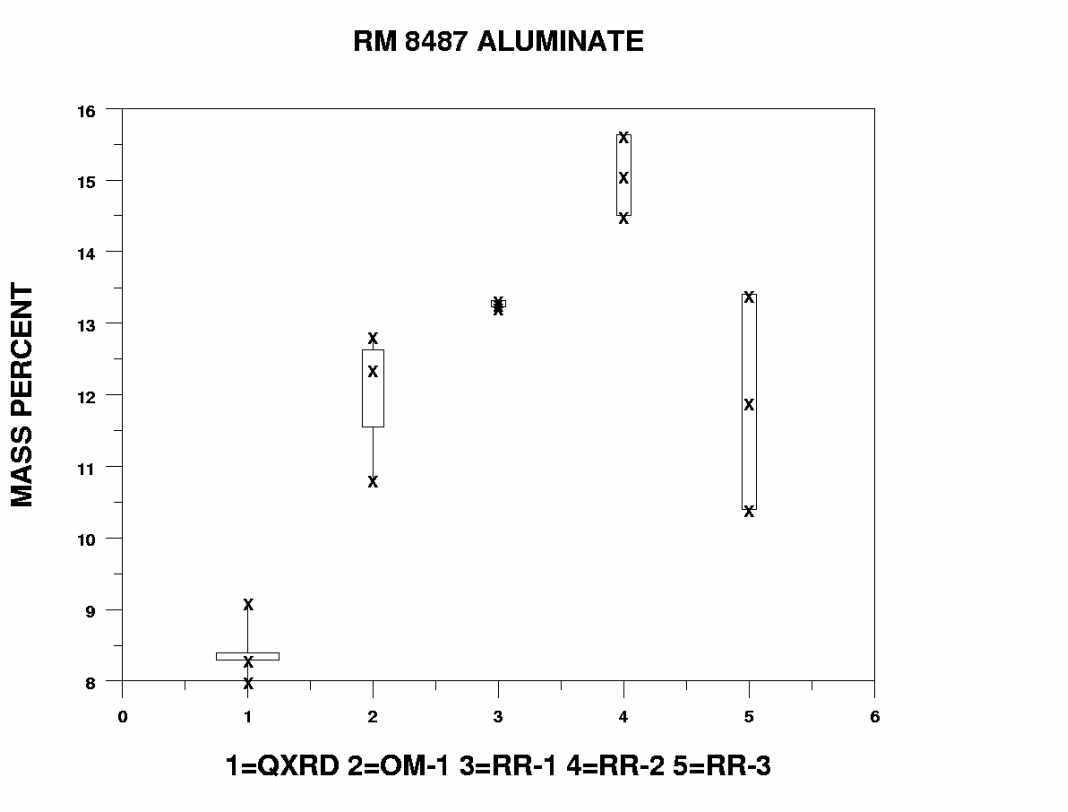

Figure 17. Box plot for RM 8487 aluminate.

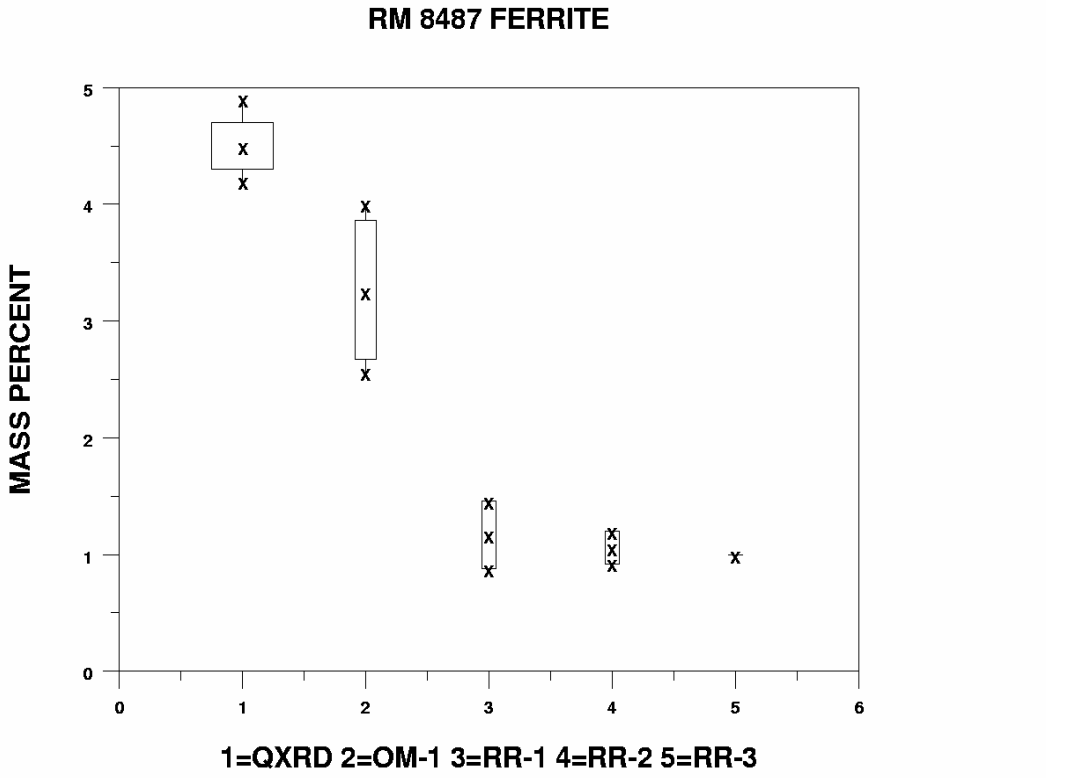

Figure 18. Box plot for RM 8487 ferrite.

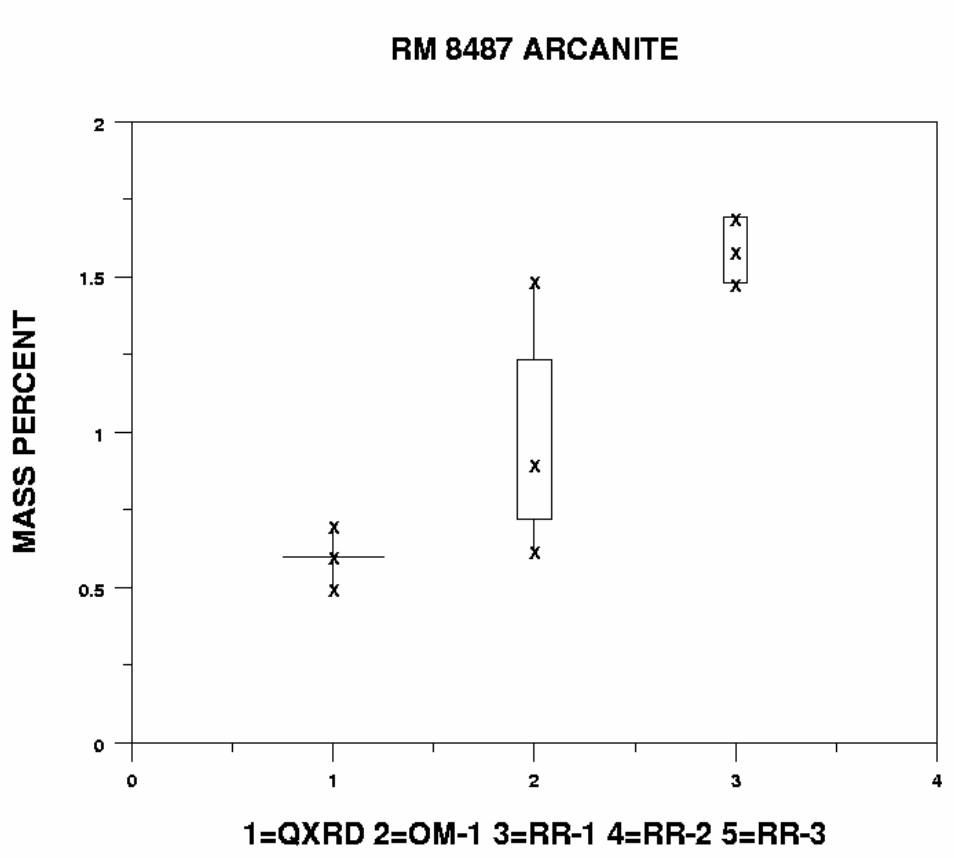

Figure 19. Box plot for RM 8487 arcanite.

RM 8488

Clinker 8488 was expected to be the easiest to characterize using optical microscopy because of its more coarsely-grained texture (Figure 19). There were two distinct interstitial phase textures though: a coarse-grained texture exhibiting large lath-like aluminate and blocky ferrite crystals, and a fine-grained texture with extremely fine-grained aluminate crystals within a fine-grained dendritic ferrite. The latter poses difficulties in resolving differences between ferrite and aluminate for optical analyses.

The silicate phases appear to show an negative correlation between the XRD and optical analyses, with XRD values of alite (Figure 20) being slightly greater and belite (Figure 21) slightly lower than the corresponding values from the optical analyses. Optical data (OM-1) show a tighter spread (interquartile range) than XRD for both silicates. This may reflect the coarse-grained nature and relative ease of identification of the silicates in this clinker.

Aluminate and ferrite values (Figures 22 and 23) demonstrate good agreement between XRD and optical data with the exception of optical round robin sets two and three. Again, this may result from the fine crystal size and resulting difficulty in observing this phase and in the experimental approach (magnification) used in performing the optical point count.

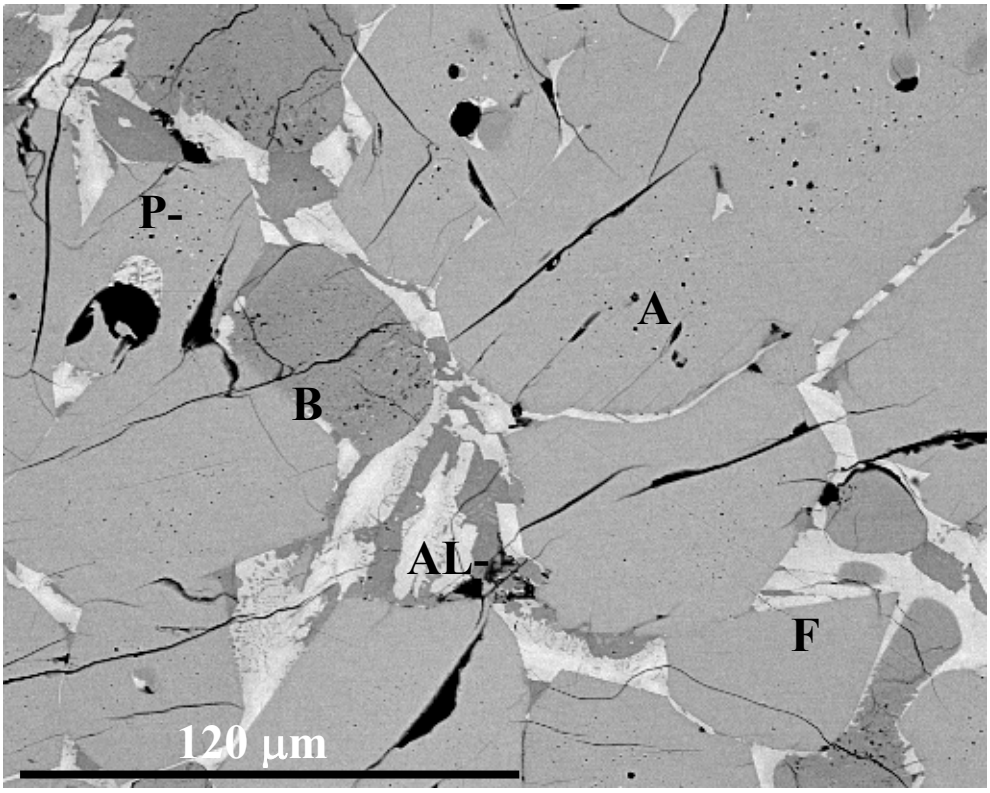

Figure 20. SEM backscattered electron image of RM 8488 showing alite (A), belite (B), aluminate (AL), ferrite (F), and porosity (P).

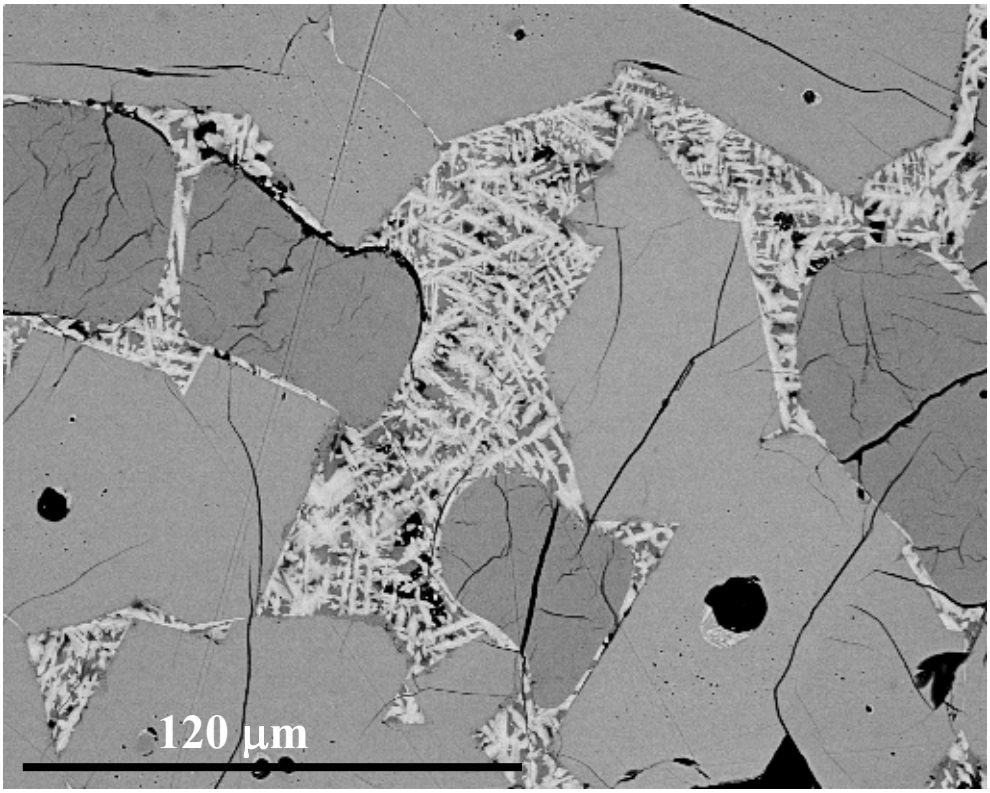

Figure 21. SEM backscattered electron image of a finer-grained interstitial phase texture in some fragments of RM 8488, which will be more difficult to point count in the microscope.

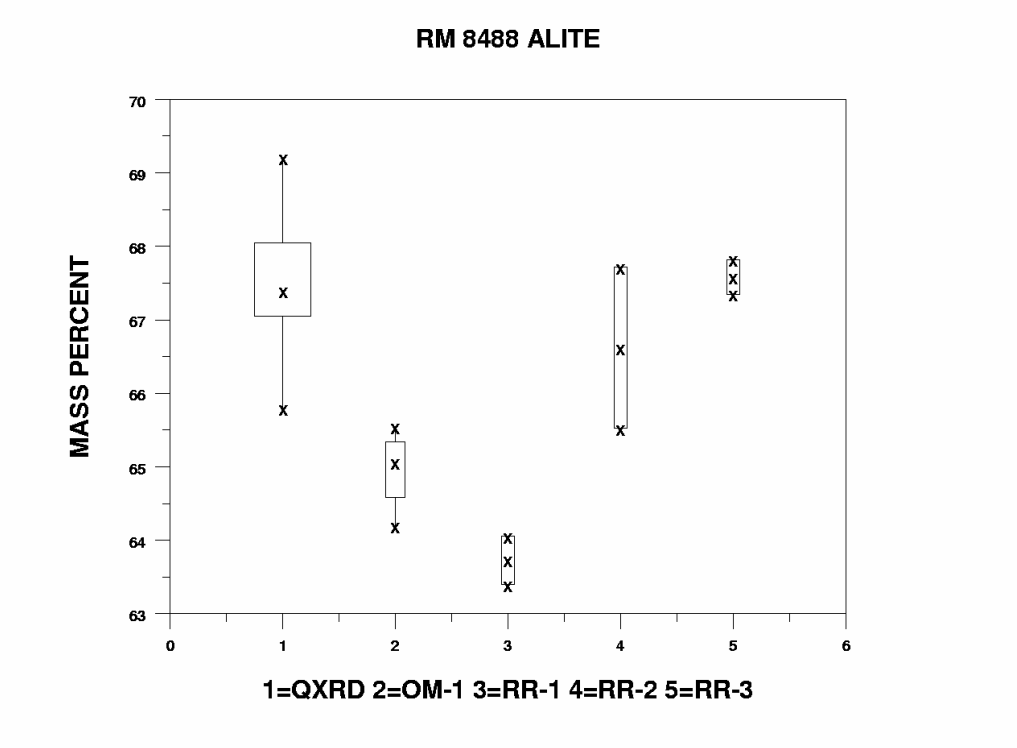

Figure 22. Box plot for RM 8488 alite.

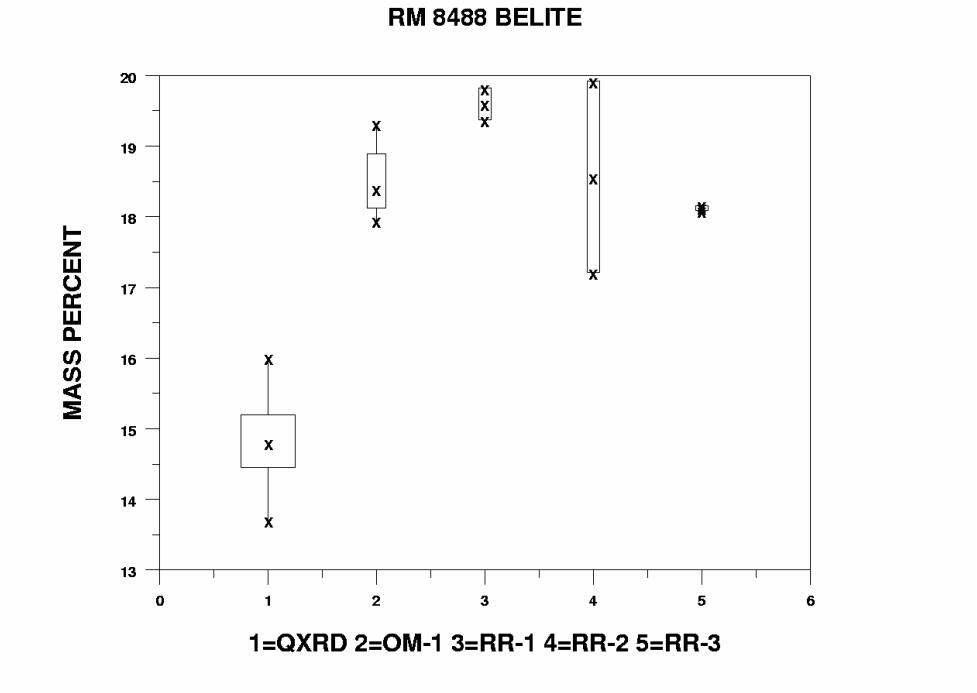

Figure 23. Box plot for RM 8488 belite.

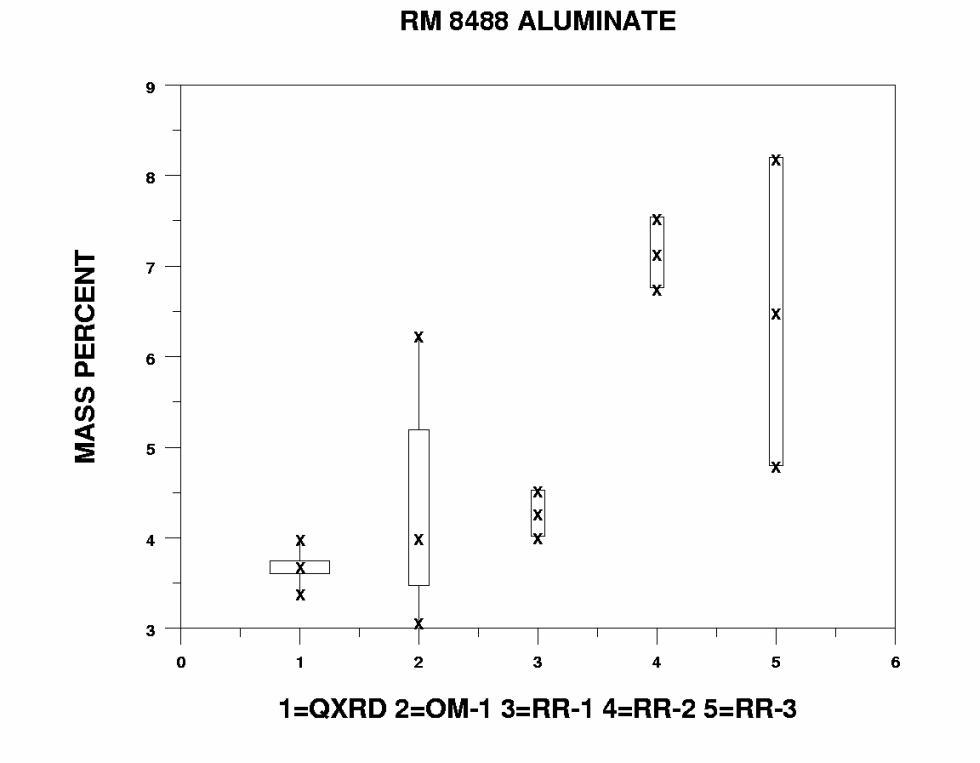

Figure 24. Box plot for RM 8488 aluminate.

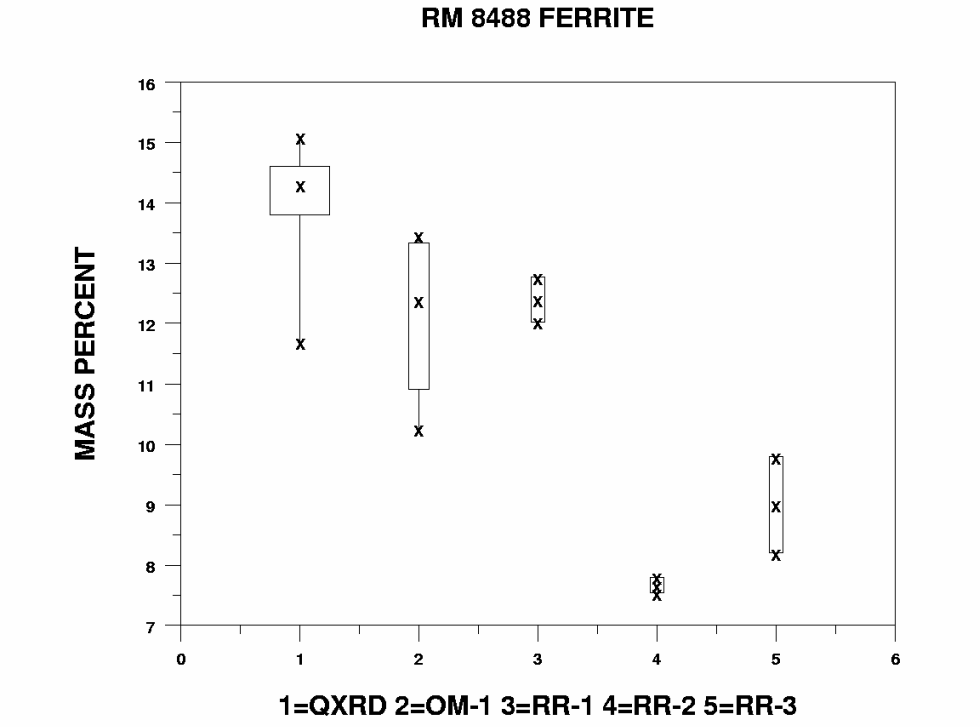

Figure 25. Box plot for RM 8488 ferrite.

Numerical Summaries: Consensus Means and Uncertainties in Phase Abundance

Often a reference material is certified based on data from more than one measurement method. This situation occurs when no single method can provide the necessary level of accuracy and/or when there is no single method whose sources of uncertainty are well understood and quantified. Measurements from different sources, different laboratories, different instruments, and different methods can exhibit significant between-method variability, as well as distinct within-method variances. A common goal in the analysis of such data is to compute a best consensus value and to attach a meaningful consensus uncertainty to that value. The results of the combined XRD and optical microscopy data sets are presented in Table 6. Three methods for combining these data sets are presented and discussed below.

The Naive Method

A naive approach [16,17] is to regard the different method results for the same analyte as being repeated estimates of a single true mean, and to compute the consensus mean as the unweighted mean of the different group means, and the consensus uncertainty as:

$$t_{(n-1)} \times \frac{(s)}{\sqrt{n}} \qquad (2)$$

where n is the number of groups, the ordinary sample standard deviation s is computed on the mean values themselves, and t is the appropriate tabulated value of the Student t percent point function for achieving 95 % confidence. A very high t value for the case n=2 ($t \approx 13$) typically precludes using this approach when only two groups are available. Otherwise, this method is useful in that it is simple, is probably something that many practitioners would attempt to use, and will often give a consensus value identical or very close to other naturally weighted methods. The naive method yields a less conservative uncertainty than those provided by other methods that take other sources of error into account, but it can serve as a baseline for those methods.

The Levenson et al. (BOB) Method: Bound on Bias

The point of departure for a new method of consensus mean/uncertainty estimation proposed by Levenson et al. at NIST [18], is that the intent of using multiple methods is to quantify systematic effects (biases) of individual methods by using the variation across the multiple methods results. However, if the number of methods is small–two to four, as is the case here–then the sample standard deviation of the method means will be a poor estimator of the uncertainty of the systematic effects. To overcome this deficiency, this method uses a Type B model [19] for the uncertainty of the systematic effects. In practice, a uniform distribution, bounded by the range of method results, has been found to be effective as a Type B model. Variants of the method make explicit use of between-method bias (or bias squared), computed as the difference between the largest group mean and smallest group mean or between the largest and grand average of the group means [20], as a proxy for between-method variance. Here we explicitly combine in quadrature an estimate of within-method variation obtained by pooling the standard errors associated with each method with an estimate of between-method variation obtained by dividing half the max-mean minus the min-mean range by the square root of three to convert to a uniform standard error.

The Mandel-Paule-Vangel-Rukhin (MPVR) Method: Maximum Likelihood Estimation

Another approach to computing consensus estimates is to get an explicit estimate of the intermethod (intergroup) variance, and sum that with a pooled estimate of the within-method (within-group) variance, using the combination to weight the contributions from the different methods to form a consensus mean. An estimation equation approach for the determination of the between-group variance developed by Mandel and Paule [21] has often been used at NIST, particularly in the certification of standard reference materials. Vangel-Rukhin [22] showed that the Mandel-Paule solution can be interpreted as an approximation to maximum likelihood. We compute the MPVR estimates of the inter method variances here and add them to a standard pooled estimates of the within method variances, take the square root to get an estimate of the overall standard errors, and multiply by an expansion factor of 2. This method has the virtues of explicitly quantifying within-group and between-group variation, and being rooted in a broadly applicable important general method of mathematical statistics, namely maximum likelihood. The drawback is that the estimation equation solution and formulations of its variance are strictly speaking only asymptotically correct, so that MPVR estimates are better for data sets where many (e.g. >10) methods/groups are present.

Comparing the consensus means and uncertainties obtained across the comparable sets of RM/analyte data, one can observe the following. Consensus means agree very well across all sets. Naive and BOB must agree because they are both unweighted means of (group) means. But the weighting scheme of MPVR (maximum likelihood) in general either doesn't move the consensus away from the unweighted mean–at least to within the reportable precision–or perturbs it only very slightly. Comparing the consensus uncertainties as calculated here, one can observe the general pattern: U(naive) < U(BOB) < U(MPVR). U(naive) is actually computed from an incorrect, or overly naive, underlying statistical model, one that assumes that all the varying groups' data come from a single parent normal population (same mean, same variance). Consequently U(naive) will, typically, lower bound the other estimates, and represents an anticonservative, and probably incorrect, estimate of the overall variation. U(BOB), on the other hand, makes no such naive population assumption, and takes explicitly into account intermethod biases. The U(BOB) estimates here represent credible consensus uncertainties. U(MPVR) estimates calculated from formula [19] of Vangel-Rukhin [22], representing confidence intervals about the consensus mean, would in fact - experience suggests - agree rather closely with the BOB estimates. However, here we have elected to combine pooled-across-group within-variance in quadrature with the MPVR estimate of between-variance, and multiply by an expansion factor of 2, to get numbers that can be thought of as representing over-conservative confidence intervals, or less-than-conservative prediction intervals for the consensus means. Because of the discrepancies among the methods clearly visible in the various box plot figures in this publication, we elect to use these slightly inflated MPVR uncertainties as the certification numbers for the respective SRM's and listed in Table 6.

Summary

Phase compositional data from X-ray powder diffraction were compared and combined with that obtained using optical microscopy for three NIST RM clinkers. Rietveld refinement of the XRD data facilitated calculation of suitable reference standards for quantitative analyses. The optical data were collected using a point-counting procedure following ASTM C 1356.

Comparison of the phase composition data sets using box plots provides a means of displaying and evaluating the data distributions, including their locations, spreads, and extremes. The data sets generally show reasonable agreement in the estimates of the individual phase abundance. The data do not always agree as well in the estimates of aluminate and ferrite. This may be the result of the fine size of the interstitial material crystals and the resulting difficulty in their microscopic identification. The XRD data generally exhibit greater precision than that of the microscopy point counts. This may reflect the homogenization of the sample as a result of the fine grinding required for XRD analyses and the larger sampling volume (about twice) for powder diffraction compared to microscopy. In the case of the microscope values for RM 8488, the coarser texture of the clinker may allow for easier phase identification.

Certification of a Reference Material is often based upon more than one measurement method. X-ray powder diffraction and microscopy analyses are the intended use of these clinkers and so were used for determining the phase abundance. To establish best consensus values and meaningful uncertainties, three methods of combining these data sets were applied. The mean values of individual phase abundance do not vary from method to method, but the 95 % uncertainty interval values do, depending upon the method.

In selecting a single method to report consensus values, the maximum likelihood (MPVR method) would be favored. The MPVR method produces a weighted mean with a weighting scheme that does not necessarily skew the consensus value in the direction of the large number of XRD values and generally produces the most conservative uncertainty interval. The MPVR method also takes explicitly into account between- as well as within-method variance. The RM clinker certificate values and uncertainties, based upon the MPVR method, are provided in Table 6.

Table 6. Combined QXRD / Optical Analyses Mean and 95 % Uncertainty Interval.

RM 8486	ALITE	BELITE	FERRITE	ALUMINATE	PERICLASE
Naive Method 2-σ	58.6 2.6	23.3 1.7	14.1* 1.0	2.3 1.7	3.3 1.2
Levenson et al. 2-σ BOB	58.6 2.8	23.3 2.2	14.1 1.1	2.3 1.5	3.3 1.4
MPVR **2-σ MLE**	**58.6** **4.0**	**23.3** **2.8**	**14.1*** **1.4**	**2.3** **2.1**	**3.3** **1.9**

***** ferrite mean and 2-σ values are based upon 2-source (XRD, OM-1) data alone.

RM 8487	ALITE	BELITE	FERRITE	ALUMINATE	PERICLASE	ARCANITE
Naive Method 2-σ	73.5 2.5	9.1 1.8	2.2 2.0	12.1 3.1	0.4 1.2	1.1 1.2
Levenson et al. 2-σ BOB	73.5 3.2	9.1 2.2	2.2 2.1	12.1 4.0	0.3 0.5	1.1 0.6
MPVR **2-σ MLE**	**73.6** **3.8**	**9.1** **2.8**	**2.2** **3.1**	**12.1** **4.9**	**0.4** **0.9**	**1.0** **1.0**

RM 8488	ALITE	BELITE	FERRITE	ALUMINATE
Naive Method 2-σ	66.1 2.1	17.9 2.3	11.0 3.2	5.2 1.9
Levenson et al. 2-σ BOB	66.1 2.4	17.9 2.9	11.0 3.8	5.2 2.3
MPVR **2-σ MLE**	**66.1** **3.4**	**17.9** **3.7**	**11.1** **5.1**	**5.0** **2.9**

Acknowledgements

The authors gratefully acknowledge the comments and suggestions of the reviewers, Chiara Ferraris, Edward Garboczi, and Leslie Struble. This work was supported by the Partnership on High Performance Concrete Technology and the Standard Reference Materials Program at the National Institute of Standards and Technology.

References

1. Kanare, H.M., "Production of Portland Cement Clinker Phase Abundance Standard Reference Materials SRMs 2686, 2687, 2688," Final Report, Construction Technology Laboratories, Skokie, IL 1987. Also see individual clinker RM certificates.

2. ASTM C 1356M - 96 Standard Test Method for Quantitative Determination of Phases in Portland Cement Clinker by Microscopical Point-Count Procedure. In Annual Book of ASTM Standards Vol. 4.01 American Society for Testing and Materials, West Conshohocken, PA 1999.

3. D.H. Campbell, Microscopical Examination and Interpretation of Portland Cement and Clinker, 2nd ed., The Portland Cement Association Research and Development Serial No. 1754, 1999, 202 pp.

4. ASTM C 1365 - 98 Standard Test Method for Determination of the Proportion of Phases in Portland Cement and Portland Cement Clinker Using X-Ray Powder Diffraction Analysis. In Annual Book of ASTM standards Vol. 4.01 American Society for Testing and Materials, West Conshohocken, PA 1999.

5 R.A. Young, ed., The Rietveld Method, International Union of Crystallography Monographs on Crystallography 5, Oxford University Press.

6. A.C. Larson and R.B. VonDreele, "GSAS General Structure Analysis System," Operational Manual, Los Alamos National Laboratory LAUR 86-748, 2000.

7. F. Nishi, Y. Takéuchi and I. Maki, "Tricalcium silicate $Ca_3O[SiO_4]$: The Monoclinic Superstructure," Zeitschrift für Kristallographie 172, 297-314 (1985).

8. P. Mondal and J.W. Jeffery, "The Crystal Structure of Tricalcium Aluminate, $Ca_3Al_2O_6$," Acta Cryst., (1975). **B31** 689.

9. K.H. Jost, B. Ziemer, and R. Seydel, "Redetermination of the Structure of α-Dicalcium Silicate, Acta Cryst. (1977) **B33**, 1696-1700.

10. A.A. Colville and S. Geller, "The Crystal Structure of Brownmillerite, Ca_2FeAlO_5," Acta Cryst. (1971) **B27**, 2311.

11. Y. Takéuchi, F. Nishi, and I. Maki, "Crystal-Chemical Characterization of the 3 CaO·Al_2O_3-Na_2O Solid Solution Series," Zeitschrift für Kristallographie 152, 259-307 (1980).

12. W.A. Klemm and J. Skalny, "Selective Dissolution of Clinker Minerals and Its Applications, Martin Marietta Technical Report 77-32, 1977, 26 pp.

13. J.C. Taylor and C.E. Matulis, "Absorption Contrast Effects in the Quantitative XRD Analysis of Powders by Full Multi-phase Profile Refinement," J. Appl. Cryst. 1991, 24, 14-17.

14. H.F.W. Taylor, Cement Chemistry, 2nd edition, Thomas Telford, London, 1997, 459 pp.

15. A. Heckert and J. J. Filliben, Dataplot Reference Manual , http://www.itl.nist.gov/div898/software/dataplot/

16. Neter, J. Kutner, M.H. Nachtsheim, C.J., Wasserman, W., APPLIED LINEAR STATISTICAL MODELS 4th edtn., Irwin/McGraw-Hill Chicago 1996.

17. Taylor, B.N. and Kuyatt, Chris E. "Guidelines for Evaluating and Expressing the Uncertainty of NIST Measurement Results," NIST Technical Note 1297 USDOC 1994.

18. M.S. Levenson D.L. Banks K.R. Eberhardt, L.M. Gill, W.F. Guthrie, H.K. Liu, M.G. Vangel, J.H. Yen, and N.F. Zhang, ``An Approach to Combining Results from Multiple Methods Motivated by ISO GUM," NIST JOUR RESEARCH vol. 105 #4, July-August 2000, pp. 571-579.

19. Guide to the Expression of Uncertainty in Measurement ISO Switzerland 1st ed. 1993.

20. S.B. Schiller and K.R. Eberhardt, "Combining data from independent chemical analysis methods" Spectrochimica Acta vol. 46B, no. 12, 1991 pp. 1607-1613.

21. Mandel, J., EVALUATION AND CONTROL OF MEASUREMENTS Marcel Dekker, New York, 1991 sections 4.4-4.5

22. Rukhin, A.L. Vangel, M.G., ``Estimation of a Common Mean and Weighted Means Statistics, "JOURNAL OF THE AMERICAN STATISTICAL ASSOCN. March 1998 Vol. 93 no. 441 pp. 303-308.

Appendix A. Structure Models for Clinker Phases

Phase: Alite **Formula:** Ca_3SiO_5 **ICDD:** 42-551

Reference: F. Nishi, Y. Takéuchi and I. Maki, "Tricalcium silicate $Ca_3O[SiO_4]$: The monoclinic superstructure," Zeitschrift für Kristallographie 172, 297-314 (1985)

Z: 36 **Space Group:** Cm **Density:** 2.935 g cm^{-3}

Cell Parameters (Å)

a	b	c	β	Vol. (Å^3)
33.3594	7.0800	18.6823	94.231	4299

Atomic Parameters

Atom	x	y	z	name	U_{iso}
Ca	0.0050	0.0000	0.0073	CA01	0.023
Ca	0.6673	0.0000	0.1746	CA02	0.023
Ca	0.3216	0.0000	0.3318	CA03	0.023
Ca	-0.0056	0.0000	0.5008	CA04	0.023
Ca	0.6636	0.0000	0.6705	CA05	0.023
Ca	0.3365	0.0000	0.8283	CA06	0.023
Ca	0.5942	0.0000	-0.0651	CA07	0.023
Ca	0.2590	0.0000	0.0908	CA08	0.023
Ca	-0.0805	0.0000	0.2656	CA09	0.023
Ca	0.5865	0.0000	0.4380	CA10	0.023
Ca	0.2568	0.0000	0.5982	CA11	0.023
Ca	-0.0742	0.0000	0.7693	CA12	0.023
Ca	0.7385	0.0000	-0.0997	CA13	0.023
Ca	0.3991	0.0000	0.0749	CA14	0.023
Ca	0.0640	0.0000	0.2465	CA15	0.023
Ca	0.7279	0.0000	0.4026	CA16	0.023
Ca	0.3994	0.0000	0.5693	CA17	0.023
Ca	0.0670	0.0000	0.7420	CA18	0.023
Ca	-0.0819	0.2833	-0.0858	CA19	0.023
Ca	0.5825	0.2538	0.0949	Ca20	0.023
Ca	0.2435	0.2503	0.2485	Ca21	0.023
Ca	-0.0913	0.2558	0.4202	Ca22	0.023
Ca	0.5764	0.2562	0.5897	Ca23	0.023
Ca	0.2452	0.2419	0.7499	Ca24	0.023
Ca	0.0052	0.2341	-0.1545	Ca25	0.023
Ca	0.6737	0.2312	0.0109	Ca26	0.023
Ca	0.3360	0.2321	0.1792	Ca27	0.023
Ca	-0.0014	0.2410	0.3453	Ca28	0.023
Ca	0.6659	0.2290	0.5122	Ca29	0.023
Ca	0.3355	0.2379	0.6788	Ca30	0.023
Ca	0.8300	0.2735	-0.0109	Ca31	0.023
Ca	0.4873	0.2512	0.1583	Ca32	0.023
Ca	0.1515	0.2702	0.3312	Ca33	0.023
Ca	0.8196	0.2641	0.4896	Ca34	0.023
Ca	0.4917	0.2808	0.6577	Ca35	0.023

Ca	0.1606	0.2712	0.8240	Ca36	0.023
Si	0.0833	0.0000	0.4288	Si1	0.007
Si	0.2384	0.0000	-0.0838	Si2	0.007
Si	0.4292	0.0000	0.7460	Si3	0.007
Si	0.5699	0.0000	0.7506	Si4	0.007
Si	-0.0943	0.0000	0.0741	Si5	0.007
Si	-0.1015	0.0000	0.5918	Si6	0.007
Si	0.0966	0.0000	-0.0851	Si7	0.007
Si	0.1637	0.0000	0.1591	Si8	0.007
Si	0.1628	0.0000	0.6629	Si9	0.007
Si	0.2340	0.0000	0.4118	Si10	0.007
Si	0.4214	0.0000	0.2509	Si11	0.007
Si	0.5008	0.0000	0.0039	Si12	0.007
Si	0.4975	0.0000	0.5004	Si13	0.007
Si	0.5682	0.0000	0.2442	Si14	0.007
Si	0.7600	0.0000	0.0882	Si15	0.007
Si	0.7563	0.0000	0.5803	Si16	0.007
Si	-0.1748	0.0000	0.3338	Si17	0.007
Si	-0.1693	0.0000	-0.1575	Si18	0.007
O	0.9900	0.0000	0.2450	O1a	0.022
O	0.9880	0.0000	0.2450	O1b	0.022
O	0.0380	0.0000	0.1190	O2a	0.022
O	0.0520	0.0000	0.1240	O2b	0.022
O	0.0300	0.0000	0.5990	O3a	0.022
O	0.0380	0.0000	0.6100	O3b	0.022
O	-0.0040	0.0000	0.7530	O4a	0.022
O	-0.0050	0.0000	0.7540	O4b	0.022
O	0.3720	0.0000	-0.0770	O5a	0.022
O	0.3730	0.0000	-0.0470	O5b	0.022
O	0.3290	0.0000	0.0750	O6a	0.022
O	0.3310	0.0000	0.0770	O6b	0.022
O	0.2890	0.0000	0.2110	O7a	0.022
O	0.2890	0.0000	0.2230	O7b	0.022
O	0.3620	0.0000	0.4410	O8a	0.022
O	0.3620	0.0000	0.4420	O8b	0.022
O	0.3250	0.0000	0.5830	O9a	0.022
O	0.3340	0.0000	0.5950	O9b	0.022
O	0.2820	0.0000	0.7240	O10a	0.022
O	0.2930	0.0000	0.7320	O10b	0.022
O	0.6660	0.0000	-0.0930	O11a	0.022
O	0.6750	0.0000	-0.0810	O11b	0.022
O	0.6270	0.0000	0.0490	O12a	0.022
O	0.6340	0.0000	0.0670	O12b	0.022
O	0.7060	0.0000	0.2850	O13a	0.022
O	0.7040	0.0000	0.2900	O13b	0.022
O	0.6480	0.0000	0.4210	O14a	0.022
O	0.6550	0.0000	0.4140	O14b	0.022
O	0.6080	0.0000	0.5640	O15a	0.022
O	0.6220	0.0000	0.5670	O15b	0.022
O	0.7050	0.0000	0.7630	O16a	0.022

O	0.7090	0.0000	0.7710	O16b	0.022
O	0.9490	0.0000	0.3760	O17a	0.022
O	0.9570	0.0000	0.4010	O17b	0.022
O	0.9600	0.0000	0.8970	O18a	0.022
O	0.9650	0.0000	0.9070	O18b	0.022
O	0.1110	0.0000	0.3570	D11	0.018
O	0.0350	0.0000	0.4080	D12	0.018
O	0.0960	0.1870	0.4740	D13	0.018
O	0.2150	0.0000	-0.0110	U24	0.018
O	0.2860	0.0000	-0.0630	U25	0.018
O	0.2260	0.1840	-0.1330	U26	0.018
O	0.4500	0.0000	0.6680	D31	0.018
O	0.3790	0.0000	0.7300	D32	0.018
O	0.4430	0.1830	0.7910	D33	0.018
O	0.5490	0.0000	0.8300	U44	0.018
O	0.6160	0.0000	0.7670	U45	0.018
O	0.5550	0.1880	0.7040	U46	0.018
O	-0.1180	0.0000	0.1490	U54	0.018
O	-0.0440	0.0000	0.0930	U55	0.018
O	-0.1070	0.1870	0.0270	U56	0.018
O	-0.1230	0.0000	0.6690	U64	0.018
O	-0.0540	0.0000	0.6080	U65	0.018
O	-0.1170	0.1860	0.5420	U66	0.018
O	0.1190	0.0000	-0.1610	D71	0.018
O	0.0480	0.0000	-0.1030	D72	0.018
O	0.1100	0.1890	-0.0380	D73	0.018
O	0.0740	0.0000	-0.0090	U74	0.018
O	0.0550	0.0000	-0.1380	U75	0.018
O	0.1250	0.1890	-0.0730	U76	0.018
O	0.1410	0.0500	0.0800	G81	0.018
O	0.1340	-0.1230	0.2080	G82	0.018
O	0.2050	-0.1230	0.1510	G83	0.018
O	0.1760	0.1970	0.2020	G84	0.018
O	0.1850	0.0000	0.5870	D91	0.018
O	0.1140	0.0000	0.6450	D92	0.018
O	0.1760	0.1890	0.7100	D93	0.018
O	0.1400	0.0000	0.7390	U94	0.018
O	0.2120	0.0000	0.6810	U95	0.018
O	0.1410	0.1890	0.6270	U96	0.018
O	0.1400	0.0500	0.5840	G91	0.018
O	0.1330	-0.1230	0.7120	G92	0.018
O	0.2040	-0.1230	0.6550	G93	0.018
O	0.1750	0.1970	0.7060	G94	0.018
O	0.2550	0.0000	0.3350	D101	0.018
O	0.2680	0.0000	0.4800	D102	0.018
O	0.2060	0.1890	0.4150	D103	0.018
O	0.2120	0.0000	0.4870	D104	0.018
O	0.2830	0.0000	0.4300	D105	0.018
O	0.2210	0.1890	0.3650	D106	0.018
O	0.4440	0.0000	0.1750	D111	0.018

```
O     0.3720    0.0000    0.2330  D112   0.018
O     0.4350    0.1891    0.2980  D113   0.018
O     0.3990    0.0000    0.3270  U114   0.018
O     0.3820    0.0000    0.1930  U115   0.018
O     0.4500    0.1890    0.2570  U116   0.018
O     0.4780    0.0000    0.0080  U124   0.018
O     0.5500    0.0000    0.2200  U125   0.018
O     0.4870    0.1890   -0.0430  U126   0.018
O     0.4780    0.0500   -0.0750  G121   0.018
O     0.4660   -0.1230    0.0400  G122   0.018
O     0.5420   -0.1230   -0.0040  G123   0.018
O     0.5130    0.1970    0.0470  G124   0.018
O     0.5200    0.0000    0.4250  D131   0.018
O     0.4480    0.0000    0.4830  D132   0.018
O     0.5110    0.1890    0.5470  D133   0.018
O     0.5200    0.0500    0.5800  G131   0.018
O     0.5260   -0.1280    0.4510  G132   0.018
O     0.4560    0.1230    0.5080  G133   0.018
O     0.4810    0.1970    0.4630  G134   0.018
O     0.5910    0.0000    0.1690  D141   0.018
O     0.6020    0.0000    0.3120  D142   0.018
O     0.5400    0.1890    0.2480  D143   0.018
O     0.5460    0.0000    0.3200  U144   0.018
O     0.6170    0.0000    0.2620  U145   0.018
O     0.5550    0.1890    0.1970  U146   0.018
O     0.7820    0.0000    0.0130  D151   0.018
O     0.7110    0.0000    0.0700  D152   0.018
O     0.7730    0.1890    0.1350  D153   0.018
O     0.7380    0.0000    0.1640  U154   0.018
O     0.7260    0.0000    0.0200  U155   0.018
O     0.7880    0.1890    0.0850  U156   0.018
O     0.7880    0.0000    0.5050  D161   0.018
O     0.7070    0.0000    0.5650  D162   0.018
O     0.7690    0.1910    0.6260  D163   0.018
O     0.7340    0.0000    0.6560  U164   0.018
O     0.7170    0.0000    0.5220  U165   0.018
O     0.7870    0.1800    0.5940  U166   0.018
O    -0.1970    0.0000    0.4090  U174   0.018
O    -0.1260    0.0000    0.3520  U175   0.018
O    -0.1880    0.1890    0.2870  U176   0.018
O    -0.1970    0.0500    0.2550  G171   0.018
O    -0.2040   -0.1230    0.3830  G172   0.018
O    -0.1340   -0.1230    0.3260  G173   0.018
O    -0.1630    0.1970    0.3770  G174   0.018
O    -0.1520    0.0500    0.4130  G175   0.018
O    -0.1450   -0.1230    0.2850  G176   0.018
O    -0.2160   -0.1230    0.3420  G177   0.018
O    -0.1870    0.1970    0.2910  G178   0.018
O    -0.1920    0.0000   -0.0820  U184   0.018
O    -0.1200    0.0000   -0.1400  U185   0.018
```

```
O    -0.1830    0.1890   -0.2040  U186   0.018
O    -0.1920    0.0500   -0.2370  G181   0.018
O    -0.1990   -0.1230   -0.1080  G182   0.018
O    -0.1280   -0.1230   -0.1650  G183   0.018
O    -0.1580    0.2100   -0.1250  G184   0.018
```

Phase: β-Dicalcium Silicate (larnite) **Formula:** Ca_2SiO_4 **ICDD:** 33-302

Reference: K.H. Jost, B. Ziemer and R. Seydel "Redetermination of the Structure of β-Dicalcium Silicate," *Acta Cryst.* (1977). **B33,** 1696-1700

Z: 4 **Space Group:** $P2_1/n$ **Density:** 3.326 g cm^{-3}

Cell Parameters (Å)

a	b	c	β	Vol. (Å^3)
5.502	6.745	9.297	94.59°	343.9

Atomic Parameters

	x	y	z	U_{iso}
Ca(1)	0.2738	0.3428	0.5694	0.004813
Ca(2)	0.2798	0.9976	0.2981	0.003800
Si	0.2324	0.7841	0.5817	0.002406
O(1)	0.2864	0.0135	0.5599	0.011525
O(2)	0.0202	0.7492	0.6919	0.008486
O(3)	0.4859	0.6682	0.6381	0.007979
O(4)	0.1558	0.6710	0.4264	0.007852

Phase: Brownmillerite (C_4AF) **Formula:** Ca_2FeAlO_5 **ICDD:** 30-226

Reference: A.A. Colville and S. Geller, "The Crystal Structure of Brownmillerite, Ca_2FeAlO_5," Acta Cryst. (1971) B27, 2311

Space Group: Ibm2 **Z:** 4 **Density:** 3.683 g cm^{-3}

Cell Parameters (Å)

a	b	c	Vol.(Å^3)
5.584	14.60	5.374	438.12

Atomic Parameters

	x	y	z	Occ.
Ca	0.0273	0.1087	0.4920	1.00
Fe	0.0	0.0	0.0	0.76
Al	0.0	0.0	0.0	0.24
Al	0.9283	0.2500	0.9533	0.76
Fe	0.9283	0.2500	0.9533	0.24
O	0.2523	0.9861	0.2491	1.00
O	0.0680	0.1439	0.0246	1.00
O	0.8607	0.2500	0.6193	1.00

Vibrational Parameters

	U_{11}	U_{22}	U_{33}	U_{12}	U_{13}	U_{23}
Ca	0.004500	0.000800	0.007900	0.001000	-0.000200	0.000000
Fe	0.001500	0.011000	0.002900	0.000000	0.000000	0.000000
Al	0.001500	0.011000	0.002900	0.000000	0.000000	0.000000
Al	0.001200	0.000400	0.002500	0.000000	-0.000700	0.000000
Fe	0.001200	0.000400	0.002500	0.000000	-0.000700	0.000000
O	0.002700	0.001100	0.006900	-0.000500	-0.000200	-0.000600
O	0.005500	0.001200	0.002200	0.000600	-0.001600	0.000200
O	0.003600	0.000200	0.007400	0.000000	-0.000700	0.000000

Phase: Tricalcium Aluminate **Formula:** $Ca_3Al_2O_6$ **ICDD:** 38-1429

Reference: P. Mondal and J.W. Jeffery, "The Crystal Structure of Tricalcium Aluminate, $Ca_3Al_2O_6$", *Acta Cryst.* (1975). **B31,** 689.

Space Group: Pa3 **Z:** 24 **Density:** 3.027 g cm^{-3}
Cell Parameters (Å) a 15.263 **Vol (Å^3):** 3556

Atomic Parameters

	x	y	z
Ca(1)	0.0000	0.0000	0.0000
Ca(2)	0.5000	0.0000	0.0000
Ca(3)	0.2561	0.2561	0.2561
Ca(4)	0.3750	0.3750	0.3750
Ca(5)	0.1386	0.3763	0.1272
Al(1)	0.2526	0.0133	0.0197
Al(2)	0.2444	0.2335	0.0046
O(1)	0.2777	0.1241	0.0103
O(2)	0.4835	0.1315	0.2536
O(3)	0.2664	0.2841	0.1049
O(4)	0.2350	0.4047	0.2921
O(5)	0.3491	-0.0385	-0.0174
O(6)	0.1500	-0.0104	-0.0242

Vibrational Parameters

	U_{11}	U_{22}	U_{33}	U_{32}	U_{31}	U_{21}
Ca(1)	0.0060	0.0060	0.0060	0.0280	0.0280	0.0280
Ca(2)	0.0084	0.0084	0.0084	0.0001	-0.0001	0.0001
Ca(3)	0.0079	0.0079	0.0079	0.0013	0.0013	0.0013
Ca(4)	0.0117	0.0117	0.0117	0.0027	0.0027	0.0027
Ca(5)	0.0079	0.0090	0.0223	-0.0010	0.0051	0.0026
Ca(6)	0.0060	0.0092	0.0096	-0.0011	0.0023	0.0011
Al(1)	0.0056	0.0058	0.0080	-0.0022	-0.0003	-0.0011
Al(2)	0.0078	0.0059	0.0065	-0.0011	0.0015	0.0009
O(1)	0.0170	0.0097	0.0176	-0.0002	-0.0025	-0.0390
O(2)	0.1380	0.0086	0.0188	-0.0039	0.0014	-0.0013
O(3)	0.0083	0.0159	0.0147	0.0044	-0.0062	-0.0081
O(4)	0.0142	0.0094	0.0191	-0.0011	0.0770	0.0054
O(5)	0.0090	0.0159	0.0147	0.0044	-0.0062	-0.0081
O(6)	0.0066	0.0154	0.0142	0.0062	0.0047	0.0010

Phase: Tricalcium Aluminate, Orthorhombic **Formula:** $Na_{2x}Ca_{3-x}Al_2O_6$ **ICDD:** 32-150

Reference: Yoshio Takéuchi and Fumito Nishi, "Crystal-chemical characterization of the 3 CaO · Al_2O_3-Na_2O solid-solution series," Zeitschrift für Kristollographie 152, 259-307 (1980), pp. 259-307

Space Group: Pbca, **Z:** 4 **Density:** 2.555 g cm^{-3}

Cell Parameters (Å)

a	**b**	**c**	**Vol. (Å^3)**
10.879	10.845	15.106	3564.5 x 0.5

Atomic Parameters

	x	**y**	**z**	**U_{iso}**	**Occupancy**
Ca1	0.00260	0.00230	0.51866	0.013425	1.0
Ca2	-0.00300	0.01680	0.24027	0.010639	1.0
Ca3	0.00873	0.26471	0.13216	0.010639	1.0
Ca4	0.25522	0.27092	0.25253	0.141850	1.0
Ca5	0.26315	0.24684	0.49821	0.013045	.696 Ca, .304 Na
Na	0.00260	-0.01560	-0.00730	0.035716	1.0
Al1	-0.00430	-0.21416	0.11621	0.006966	.888 Al, .061 Fe, .051 Si
Al2	0.23742	-0.00420	0.11250	0.007219	.868 Al, .072 Fe, .060 Si
Al3	0.24050	0.00420	-0.10879	0.007979	.831 Al, .092 Fe, .077 Si
O1	-0.14470	-0.13520	0.11010	0.020391	1.0
O2	0.11420	-0.10520	0.13130	0.022924	1.0
O3	0.28570	-0.02580	0.00170	0.015578	1.0
O4	-0.01250	-0.28660	0.21780	0.023177	1.0
O5	0.02150	-0.29420	0.01800	0.017985	1.0
O6	0.35710	-0.07150	0.17160	0.016845	1.0
O7	0.19040	0.14770	0.13140	0.017605	1.0
O8	0.16380	-0.12810	-0.14440	0.015198	1.0
O9	0.37220	0.06720	-0.15800	0.016085	1.0

Phase: Arcanite **Formula:** K_2SO_4 **ICDD:** 5-613
Reference: R.T. Robinson, "The Crystal Structure of β-K_2SO_4 and of β-K_2PO_3F," J. Phys. Chem., Vol. 62, August, 1958, pp. 925-928.

Space Group: Pnam **Z**=4 **Density:** 2.666 g cm^{-3}

Cell Parameters (Å)

a	b	c	**Vol.(Å^3)**
6.456	10.080	5.776	434.104

Atomic Parameters

	x	y	z	Occupancy		U_{iso}
K	0.176800	0.081800	0.250000	1.00	K1	0.017731
K	-0.011500	0.704600	0.250000	1.00	K2	0.017731
S	0.235800	0.415500	0.250000	1.00	S3	0.017731
O	0.031500	0.403200	0.250000	1.00	O4	0.017731
O	0.297000	0.557900	0.250000	1.00	O5	0.017731
O	0.299700	0.348400	0.041000	1.00	O6	0.017731

Phase: Periclase **Formula:** MgO **ICDD:** 4-829

Reference: R.W. G. Wyckoff, Crystal Structures, 2nd ed., Interscience Publishers, New York, 1963

Space Group: Fm-3m **Z**=1 **Density**: 3.582 g cm^{-3}

Cell Parameters (Å) **Vol.(Å^3)**

a 4.2117	74.7

Atomic Parameters

	x	y	z	Occupancy		U_{iso}
MG	0.000000	0.000000	0.000000	1.00	MG1	0.016229
O	0.500000	0.500000	0.500000	1.00	O2	-0.001858

Phase: Lime **Formula:** CaO **ICDD:** 37-1497

Reference: R.W. G. Wyckoff, Crystal Structures, 2nd ed., Interscience Publishers, New York, 1963

Space Group: Fm-3m **Z**=1 **Density**: 3.346 g cm^{-3}

Cell Parameters (Å) **Vol.(Å^3)**

A 4.8109	111.319

Atomic Parameters

	x	y	z	Occupancy		U_{iso}
Ca	0.000000	0.000000	0.000000	1.00	Ca1	0.013803
O	0.500000	0.500000	0.500000	1.00	O2	-0.000121

Appendix B: Selective Extractions for Clinker and Cement

Salicylic Acid/Methanol Extraction (SAM)

The SAM extraction dissolves alite, belite, and free lime leaving a residue of interstitial phases aluminate and ferrite as well as periclase, alkali sulfates, and for cements, calcium sulfates. Concentration aids qualitative and quantitative analysis by reducing diffraction peak overlaps from the silicates and increases the diffraction intensities of the phases in the residue. Performing this extraction on a cement that has not been heat-treated preserves the calcium sulfate addition forms (gypsum, bassanite, and anhydrite).

The SAM solution consists of 20 g of salicylic acid in 300 ml of methanol. Stir about 5 g of powdered clinker or cement in a stoppered flask containing 300 ml of SAM solution for about 2 h. Allow the suspension to settle for about 15 min then vacuum filter using a 0.45 μm filter and Buchner funnel. Wash the residue with methanol, dry at 100 °C, and store in a vacuum desiccator. Measuring the mass loss allows the QXRD values to be re-calculated on a whole-sample basis and provides an additional estimate for total silicate content.

Potassium Hydroxide/Sugar Extraction (KOH/Sugar)

The KOH/sugar extraction dissolves the interstitial phases of aluminate and ferrite leaving a residue of silicates and minor phases. First, prepare an extraction solution with 7.5 g of KOH and 7.5 g of sucrose in 75 ml of distilled water. Stir 2.25 g of powdered clinker or cement (*heat-treated cement*) into a 95 °C KOH/sugar solution for 1 min. Filter the solution using a 0.45 μm filter and Buchner funnel, wash residue with 12 ml of water followed by 25 ml of methanol, dry residue at 100 °C, and store in a vacuum desiccator.

This extraction has the propensity to be difficult to filter. Maintaining the suspension at 95 °C while filtering may reduce this problem as does the use of a larger diameter filter paper. In more difficult cases, extraction of cement that has not been ground beyond that from the manufacturer may allow for a successful extraction. The mass loss is not measured for this extraction as the SAM extraction data are generally sufficient.

Nitric Acid/Methanol Extraction

This extraction dissolves the silicates and aluminates leaving a residue of ferrite and (if present) periclase. The extraction solution is 7 % nitric acid in methanol. Ten grams of ground clinker or cement are stirred in to 500 ml of the nitric acid/methanol solution for 30 min. The residue is then filtered, rinsed with pure methanol, dried, and stored in a vacuum desiccator. Mass loss is generally not measured for this extraction.